Evaluation of variability in GOME-2 total water vapor and nitrogen dioxide columns associated with natural oscillations

Kostas Eleftheratos[a,b], Charilaos Benetatos[a], Pieter Valks[c], Patrick Jöckel[d], Luca Lelli[e], Christos Zerefos[b,f,g,h]

[a]Department of Geology and Geoenvironment, National and Kapodistrian University of Athens, 15784 Athens, Greece

[b]Biomedical Research Foundation of the Academy of Athens, Soranou Efesiou 4, 11527 Athens, Greece

[c]EUMETSAT, Eumetsat-Allee 1, 64295 Darmstadt, Germany

[d]Institut für Physik der Atmosphäre (IPA), Deutsches Zentrum für Luft- und Raumfahrt (DLR), 82234 Oberpfaffenhofen, Germany

[e]Institut für Methodik der Fernerkundung (IMF), Deutsches Zentrum für Luft- und Raumfahrt (DLR), 82234 Oberpfaffenhofen, Germany

[f]Research Centre for Atmospheric Physics and Climatology, Academy of Athens, Vasilissis Sofias 79, 11521 Athens, Greece

[g]Mariolopoulos-Kanaginis Foundation (MKF) for the Environmental Sciences, Patriarchou Ioakim 30-32, 10675 Athens, Greece

[h]Navarino Environmental Observatory (N.E.O.), Costa Navarino, 24001 Messinia, Greece

Corresponding author: Dr. Kostas Eleftheratos, kelef@geol.uoa.gr

Early Online Release: This preliminary version has been accepted for publication in *Journal of Climate*, may be fully cited, and has been assigned DOI 10.1175/JCLI-D-24-0730.1. The final typeset copyedited article will replace the EOR at the above DOI when it is published.

ABSTRACT

This study presents the variability of total water vapor (H_2O) and nitrogen dioxide (NO_2) columns associated with natural oscillations (QBO, ENSO, NAO), based on monthly GOME-2 Level-3 trace gas column data produced under the ACSAF project. The periods studied are 01/2007-12/2018 for GOME-2A, 01/2013-05/2025 for GOME-2B and 01/2019-05/2025 for GOME-2C. The QBO-type periodicity in total NO_2 is strongest in the tropics with a measurable amplitude of a few percent. Going from low to mid-latitudes, there is a phase shift in the QBO impact seen in total NO_2. Variability of total H_2O is not significantly correlated with the QBO. The effects of ENSO on total H_2O are clearly seen in the tropics, while the effect of NAO is evident in the northern midlatitudes. Variability in total H_2O from GOME-2 in regions affected by ENSO and NAO is compared with that from CAMS reanalysis and ECHAM/MESSy Atmospheric Chemistry (EMAC) model results, and good agreement is found between the datasets. Overall, our results show that the total column NO_2 and H_2O data from GOME-2 capture well the variability associated with large-scale natural fluctuations in the recent past, supporting that QBO/ENSO/NAO–tracer correlations can serve as a diagnostic tool for model and reanalysis evaluations. This provides confidence that data from the newer versions of the GOME-2 instrument (GOME-2B, GOME-2C) can be quite useful for monitoring the response of NO_2 and H_2O to potential anomalies in the QBO/ENSO/NAO signals in the near future and can significantly help in evaluating the representation of these natural cycles in climate model simulations of trace gases in the coming years.

SIGNIFICANCE STATEMENT

Quasi-Biennial Oscillation, El Niño Southern Oscillation, and North Atlantic Oscillation, are known natural fluctuations that affect meteorological and climatic variables around the world. Here, we examine the ability of water vapor and nitrogen dioxide total column retrievals from the Global Ozone Monitoring Experiment–2 satellite instrument to capture variability associated with these natural perturbations and use this information to evaluate chemistry-climate model simulations and reanalysis data from the Copernicus Atmosphere Monitoring Service. Our findings indicate that the newer

versions of the Global Ozone Monitoring Experiment–2 can be quite useful for monitoring the response of total column nitrogen dioxide and water vapor to potential anomalies or changes in the signals of these natural oscillations in the near future and can significantly help to improve our knowledge for better representation of these natural oscillations in future climate model simulations of trace gases.

1. Introduction

The European Organisation for the Exploitation of Meteorological Satellites (EUMETSAT) Atmospheric Composition Satellite Application Facility (AC SAF) provides high-quality data products of total ozone and other trace gas total columns such as water vapor (H_2O), nitrogen dioxide (NO_2), sulfur dioxide (SO_2), bromine monoxide (BrO) and formaldehyde (HCHO). The data come from measurements by the Global Ozone Monitoring Experiment (GOME)-2 instruments on the polar-orbiting Meteorological Operational (MetOp) satellites (MetOp-A, MetOp-B and MetOp-C) (Hassinen et al., 2016), and contribute to studies related to the Earth's atmosphere, specifically its composition. More specifically, GOME-2 data have been used in studies investigating total and tropospheric ozone column variability and changes (Loyola et al., 2009; van der A et al., 2010; Safieddine et al., 2013; Coldewey-Egbers et al., 2014; Valks et al., 2014; Gaudel et al., 2018; Eleftheratos et al., 2019), in studies examining anthropogenic and volcanic SO_2 variations (Loyola et al., 2008; Rix et al., 2012; Brenot et al., 2014; Koukouli et al., 2016; Zerefos et al., 2017), in studies analyzing changes in total and tropospheric NO_2 columns (Safieddine et al., 2013; Liu et al., 2019; Liu et al., 2020; Liu et al., 2021), and in total H_2O (Grossi et al., 2015; Kalakoski et al., 2016; Chan et al., 2020), total BrO (Theys et al., 2009) and total HCHO studies (De Smedt et al., 2015). In addition, the data have been used in validation studies of total ozone (Scannell et al., 2012; Chiou et al., 2014; Hao et al., 2014; Boynard et al., 2018; Keppens et al., 2018; Garane et al., 2019), and total and tropospheric NO_2 (Valks et al., 2011; Pinardi et al., 2020).

In this study we focus on total H_2O and NO_2 columns from the GOME-2 instruments. Grossi et al. (2015) compared total column water vapor measurements from GOME-2

MetOp-A with respective measurements from MetOp-B as well as with data from the European Centre for Medium-Range Weather Forecasts (ECMWF) ERA-Interim analysis, Special Sensor Microwave Imager/Sounder (SSMIS) satellite measurements and the combined Special Sensor Microwave/Imager- MEdium Resolution Imaging Spectrometer (SSM/I-MERIS) satellite data. Their study identified a very good agreement between GOME-2 total columns and all three data sets, especially for land areas, although some discrepancies over ocean and over land areas with high humidity or a relatively large surface albedo were observed (Grossi et al., 2015). Kalakoski et al. (2016) validated GOME-2/MetOp total H_2O column with radiosonde data from the Integrated Global Radiosonde Archive (IGRA) archive and Global Positioning System (GPS) data from the Constellation Observing System for Meteorology, Ionosphere, and Climate (COSMIC)/SuomiNet network. The analysis showed good agreement, with high correlation coefficients between GOME-2 and the ground-based datasets (>0.9), small negative differences of GOME-2 against radiosonde and positive differences against GPS. Chan et al. (2020) developed a new total column H_2O retrieval algorithm in the visible blue spectral band for the GOME-2 instruments. The new algorithm was applied to GOME-2A and GOME-2B observations and the retrieved data in the blue band compared well with those retrieved in the red spectral band, sun photometers and radiosonde measurements. All these studies point to the correct measurements of total H_2O column by the GOME-2 instruments, however variability in GOME-2 total H_2O related to natural fluctuations was not assessed in those studies. The same also holds for total NO_2 from GOME-2. The NO_2 studies mentioned above validated NO_2 column retrievals from GOME-2 but did not assess the ability of GOME-2 NO_2 column retrievals to capture variability related to known natural oscillations.

Quasi Biennial Oscillation (QBO), El Niño Southern Oscillation (ENSO), and North Atlantic Oscillation (NAO) are low-frequency known natural oscillations in the climate system. By affecting atmospheric circulation patterns, they are expected to affect the transport and distribution of NO_2 in the atmosphere and, therefore, the total NO_2 column. However, given the very short lifetime of NO_2 (Lange et al., 2022 estimate the lifetime of NOx to be 2 to 8 hours depending on latitude), low-frequency oscillations are not thought to directly affect NO_2 concentrations and distribution, but indirectly, through chemical

processes within the NOy family. Zawodny and McCormick (1991) noted that the observed QBO features in NO_2 differ significantly from those of ozone, particularly the behavior of the NO_2 column abundances, and can be understood in light of relevant photochemistry to be due to the transport of the long-lived NOy family. This family includes various reactive nitrogen species, among which are nitric oxide (NO) and NO_2, known as NOx ($NO + NO_2$, e.g. Brohede et al., 2008; Park et al., 2017). The main source of NOx in the stratosphere is nitrous oxide (N_2O) emitted from the surface (Ravishankara et al., 2009). The oxidation of N_2O by electronically excited $O(^1D)$ atoms leads to the production of NO in the stratosphere, which is then oxidized to NO_2. These two gases (NO, NO_2) then participate in an important set of photochemical reactions that catalytically destroy ozone (Crutzen, 1979).

The relationships between QBO and nitrogen dioxide have been discussed in previous studies, e.g. Zawodny and McCormick (1991), Chipperfield et al. (1994), Tian et al. (2006), Punge and Ciorgetta (2008), Park et al. (2017). Zawodny and McCormick (1991) presented the first satellite measurements showing a QBO signal in NO_2. They found that the QBO in NO_2 is consistent with the vertical and horizontal transport of the reactive nitrogen (NOy) family and showed that ozone (O_3) and NO_2 exhibit a QBO at extratropical latitudes, consistent with strong meridional transport into the winter hemisphere. Two-dimensional model results by Chipperfield et al. (1994) showed that there is a phase change in O_3 anomaly at 28km where ozone changes from dynamical to photochemical control, and that the main cause of the QBO signal in O_3 above 30 km is the QBO modulation of NO_2 (via modulated NOy transport). Their model reproduced the observed latitudinal structure of the QBO signals in O_3 and NO_2 and it was noted that due to the different horizontal distributions of O_3 and NOy, the ozone signal shows a clear phase change in the subtropics, while the NO_2 anomaly gives a broader signal. Tian et al. (2006) used a fully coupled chemistry-climate model (CCM) to study the QBO signals in stratospheric trace gases, particularly ozone. By diagnosing model chemical rates, the authors found that the QBO pattern in NO_2, which is largely driven by the QBO of longer-lived NOy, is the main chemical driver for the O_3 QBO around 35 km, i.e., above the O_3 phase change, rather than temperature changes. They also showed that a phase change in height may exist not only in the QBO signals of O_3, but also in the QBO

signals of other long-lived chemical species. Punge and Ciorgetta (2008) showed that CCMs can reproduce the observed QBO variations in temperature and ozone when nudged toward the observed winds. They showed in particular that the QBO signal in the transport of nitrogen oxides (NOx) plays an important role in reproducing the observed ozone QBO, which is characterized by a phase reversal slightly below the level of ozone maximum in the tropics. Park et al. (2017) quantified the relationships among O_3, NOy, and N_2O, as well as their connections with the QBO, based on satellite measurements of gaseous components and meteorological data for the period 2005–2014.

El Niño impacts on reactive trace gases in the troposphere were discussed by Loyola et al. (2006) and NAO's effect on tropospheric tracers was discussed by Christoudias et al. (2012). ENSO and NAO's effects on column-integrated water vapor have been discussed by Trenberth et al. (2005), Trent et al. (2024) and references therein. Trenberth et al. (2005) showed that the variability of precipitable water for the period 1988-2001 was dominated by the evolution of ENSO, and in particular by the structures that appeared during and after the 1997-98 El Niño event. They also found that trends in precipitable water over the oceans are generally positive. Trent et al. (2024) analyzed the total column water vapor from 28 satellite and reanalysis data products between 1979 and 2019 and presented correlations with six climate indices within the long period, among which ENSO and NAO, highlighting areas of significant positive and negative correlation and the level of agreement among the various data records. While correlations with ENSO and NAO indices have already been studied, we note that Trent et al. did not analyze GOME-2A, GOME-2B and GOME-2C separately as we have done here. They analyzed the so-called GOME evolution climate product (Beirle et al., 2018), which contains total column water vapor data from July 1995 to December 2015 from merged GOME, SCHIAMACHY and GOME-2A observations. Data beyond 2015 were not analyzed. We present data from the successor instruments of GOME-2, GOME-2B, and GOME-2C and how they capture variability related to ENSO and NAO and to what extent, which was not done in the previous studies.

The objectives of this study are: a) to examine the ability of GOME-2 total NO_2 and H_2O columns to capture variability associated with natural cycles of global and regional importance (QBO, ENSO, NAO), b) to check the consistency between the variability of

total NO_2 column from GOME-2A/2B/2C instruments during these natural oscillations, as well as the respective variability of total H_2O column, and c) to evaluate the performance of the Copernicus Atmosphere Monitoring Service (CAMS) reanalysis and the European Centre for Medium-Range Weather Forecasts – Hamburg (ECHAM)/Modular Earth Submodel System (MESSy) Atmospheric Chemistry (EMAC) CCM simulations in depicting the observed natural variability of these trace gases compared to GOME-2 satellite retrievals. We note here that we do not aim to validate the specific satellite data products, as this has been done in previous studies (e.g. Grossi et al., 2015; Chan et al., 2020; Chan et al., 2023), but to present the way they ”see” these natural oscillations as it was not shown in previous studies. We have no reason to suspect that the validated GOME-2 products may not capture the inter-annual variability associated with major climate modes, but a validated product does not necessarily mean that it will definitely capture this natural variability in the long-term anyway. We also note that we do not aim to present the correlation between trace gases and climate modes as something new, as this has been reported in previous studies as mentioned above. Similarities and differences between our results and those from previous studies are discussed in Section 3. Nevertheless, the QBO/ENSO/NAO signals in total column NO_2 and H_2O from GOME-2 and CAMS, which we analyze here, were not studied before in detail. We argue that QBO/ENSO/NAO – tracer correlations can serve as a diagnostic tool for model and reanalysis evaluations.

Therefore, the main purpose of this study is to demonstrate the ability of GOME-2 instruments to capture variability of total NO_2 and H_2O columns associated with major climate modes, and to evaluate the performance of CAMS reanalysis and EMAC CCM simulations in depicting this type of natural variability in these trace gases. In view of recent studies reporting anomalies or changes in the regular cycle of large-scale natural oscillations (Anstey et al., 2021 for QBO; Lu et al., 2025 for ENSO; Mitevski et al., 2025 for NAO), we document that data from the newer versions of the GOME-2 instrument, GOME-2B and GOME-2C, can be quite useful for examining the response of NO_2 and H_2O to potential anomalies or changes in the QBO/ENSO/NAO signals in the near future and can significantly help to improve our knowledge for better representation of these natural cycles in climate model simulations of trace gases in the coming years.

2. Data and methodology

We have analysed monthly GOME-2 Level 3 (L3) trace gas column data produced within the project of EUMETSAT, AC SAF (https://acsaf.org/) (Chan et al., 2023). The datasets that have been used (NO_2 and H_2O) have been derived from the blue visible (430–465 nm for NO_2) and the near-infrared (614–683 nm for H_2O) window and have been strictly quality filtered for cloud contamination and suboptimal retrieved columns (as per Chan et al., 2023). GOME-2A covers the period 2007-2021 but we limited the analysis to 01/2007-12/2018 to avoid erroneous data due to instrument degradation, as the instrument reached the end of its lifetime. GOME-2B data analysed in this study cover the period 01/2013-05/2025 and GOME-2C data cover the period 01/2019-05/2025. The parameters analyzed are the total water vapour (H_2O) and total nitrogen dioxide (NO_2) columns.

The study also includes the analysis of monthly total H_2O column data for the period 2003-2024 from the Copernicus Atmosphere Monitoring Service (CAMS) global reanalysis EAC4 (ECMWF Atmospheric Composition Reanalysis 4) (Inness et al., 2019). The data were downloaded from the Copernicus Atmosphere Data Store at https://ads.atmosphere.copernicus.eu/datasets/cams-global-reanalysis-eac4?tab=overview (last access: 20 October 2025) and were compared with the total H_2O data from GOME-2. Stratospheric species from CAMS, including stratospheric water vapor, were recently evaluated by Chabrillat et al. (2025). For water vapor it is shown that the model exhibits a large moist bias in the tropical lower stratosphere (below 70 hPa), with values being larger than observations by more than 50% at 100 hPa, compared to ACE-FTS (Atmospheric Chemistry Experiment – Fourier Transform Spectrometer) and Aura-MLS (Microwave Limb Sounder) data. In the tropical middle stratosphere (6–50 hPa), the model biases are smaller than 10% relative to Aura-MLS and smaller than 5% relative to ACE-FTS. In the tropical upper stratosphere (up to 1 hPa), the model exhibits negative biases with decreasing pressures, reaching underestimations of 15% relative to ACE-FTS and 20% relative to Aura-MLS. In the extratropics, the model underestimates H_2O in the upper stratosphere by about 10% relative to ACE-FTS and less than 20% relative to Aura-

MLS. Over the North Pole (30–100 hPa), the biases are within ±5%, while over the South Pole (30–100hPa), the biases are between –20% and 5%. Total column NO_2 data from CAMS were not analyzed in our study and therefore comparisons between CAMS and GOME-2 total NO_2 data are not presented here. The reason is that CAMS NO_2 cannot be considered an independent data set because it assimilates GOME-2 NO_2 and therefore any comparison between the two datasets would not be considered unbiased.

In addition, we have analyzed the RD1SD-base-01 simulation results of total NO_2 and total H_2O columns from the European Centre for Medium-Range Weather Forecasts – Hamburg (ECHAM)/Modular Earth Submodel System (MESSy) Atmospheric Chemistry (EMAC) chemistry–climate model (CCM) (Jöckel et al., 2016; Jöckel et al., 2024a; Jöckel et al., 2024b). We also analyzed the RD1SD-base-01 simulations of ozone and NO_2 with 90 model levels reaching up to 0.01 hPa (about 80 km). The simulations were performed in a specified dynamics (SD) setup, i.e. nudged by Newtonian relaxation towards ECMWF ERA-5 reanalysis data. More specifically, in the EMAC simulation we nudged the prognostic variables divergence, vorticity, temperature, and the logarithm of the surface pressure by Newtonian relaxation in spectral representation with relaxation times of 48, 6, 24, and 24 hours, respectively. The nudging is applied only above the boundary layer and up to approximately 100 hPa with transition layers below and above. Moreover, the "wave-zero" of the temperature was excluded from nudging. In addition, sea surface temperature (SST) and sea-ice concentration (SIC) from the ERA-5 reanalysis data (Hersbach et al., 2020) were prescribed. The simulations refer to the period January 1979 – December 2019 and the spatial resolution applied is 2.8° x 2.8° in latitude and longitude.

The correlations between total H_2O/NO_2 columns and QBO/ENSO/NAO have been studied with a linear regression statistical model, which has been applied to the GOME-2 satellite data, the CAMS reanalysis data and the RD1SD CCM simulation results, separately. The model has been used in previous studies (e.g. Zerefos et al., 2018; Eleftheratos et al., 2019) to study the amplitude of dynamical proxies in ozone. The linear statistical model has been applied at each grid box of the datasets, in four steps as shown below:

$$deseasonalized(t) = \alpha 1 + a_{QBO10} QBO10(t) + N_{QBO10}(t); 0 < t \leq T, \quad (1)$$

$$N_{QBO10}(t) = \alpha 2 + a_{QBO30} QBO30(t) + N_{QBO30}(t); 0 < t \leq T, \quad (2)$$

$$N_{QBO30}(t) = \alpha 3 + a_{ENSO} ENSO(t) + N_{ENSO}(t); 0 < t \leq T, \quad (3)$$

$$N_{ENSO}(t) = \alpha 4 + a_{NAO} NAO(t) + N_{NAO}(t); 0 < t \leq T, \quad (4)$$

Where, *deseasonalized(t)* are the time-series of the deseasonalized total H_2O or NO_2 column, t is the time in months, with $t = 0$ corresponding to the initial month and $t = T$ corresponding to the last month. Data were deseasonalized prior to the analysis, by removing the long-term monthly mean for each calendar month. The other terms are:

- *α1, α2, α3, α4 are the intercepts in each step respectively*,
- For QBO, we used two terms, the monthly zonal wind values (u-wind) at 10 and 30 hPa in Singapore, as given by the NASA/GSFC Atmospheric Chemistry and Dynamics Laboratory (https://acd-ext.gsfc.nasa.gov/Data_services/met/qbo/qbo.html#links). We use the abbreviations QBO10 and QBO30 for zonal winds at the equator at 10 and 30 hPa, respectively. We note here that one could also use the u-wind at a single level with lead-lag, for example at 30 hPa, but we selected to work with equatorial u-winds at 10 hPa and 30 hPa that have a phase difference of ~90 degrees, which makes them almost orthogonal. This was necessary in order to apply the two QBO indices correctly; otherwise, if the QBO indices were not orthogonal, then the analysis would be biased toward removing duplicate QBO-related variability, which would be wrong.
- For ENSO, we used the Niño anomaly 3.4 index (Niño3.4) as a proxy, as given by the National Oceanic and Atmospheric Administration (NOAA) Physics Sciences Laboratory (https://psl.noaa.gov/data/climateindices/list/). Positive values in the Niño3.4 index indicate warm (El Niño) events and negative values indicate cold (La Niña) events.

- For NAO, we used the monthly North Atlantic Oscillation (NAO) Index (PC-based), as given by Jim Hurrell at NCAR (Hurrell et al., 2024).
- *N(t)* are the monthly residuals, i.e., $N_{QBO10}(t)$ are the monthly residuals after removing correlations with zonal winds at 10 hPa, $N_{QBO30}(t)$ are the monthly residuals after removing correlations with zonal winds at 30 hPa, $N_{ENSO}(t)$ are the monthly residuals after removing correlations with the Niño3.4 index, and $N_{NAO}(t)$ are the monthly residuals after removing correlations with the NAO index.

The four steps are described as follows: Eq. 1 (step 1) is used to examine and remove possible correlations with zonal winds at 10 hPa. The residuals from Eq. 1 are then inserted into Eq. 2 (step 2) to examine and remove possible correlations with zonal winds at 30 hPa. The residuals from Eq. 2 are then inserted into Eq. 3 (step 3) to examine and remove possible correlations with ENSO. Lastly, the residuals from Eq. 3 are inserted into Eq. 4 (step 4) to examine possible correlations with the NAO. The statistical method and the results from equations 1 to 4 were thoroughly tested by applying the regressions in a different order and checking whether the residuals after each step are normally distributed. The checks showed that the distributions of the residuals are normal and that the regressions do not give different results when applied in a different order. The checks of the statistical method can be found in the Supplement of this study.

We note here a few things about the expected troposphere/stratosphere relationships of NO_2 and H_2O with the QBO, ENSO and NAO. Regarding the NO_2 column, the tropospheric portion of the NO_2 column can be large in polluted areas due to human activities (e.g. Chang et al., 2022; Bai et al., 2025), and as such, strong correlations with the natural indices are not expected in such areas. Also, since most of the NO_2 amount is in the stratosphere, a correlation between the stratospheric QBO and total NO_2 column is expected, as has been shown in previous studies (e.g. Zawodny and McCormick, 1991; Chipperfield et al., 1994; Tian et al., 2006; Punge and Ciorgetta, 2008; Park et al., 2017), but correlations with oscillations developing in the troposphere such as ENSO or NAO are expected to be smaller. ENSO and NAO's effects on tropospheric tracers have also been examined before (e.g. Loyola et al., 2006; Christoudias et al., 2012). Comparisons of our results with the previous studies are discussed in Section 3. As for the H_2O

column, any possible amount of stratospheric H_2O is so small compared to the total column, that in practice GOME-2 mainly measures the tropospheric column. To be more quantitative, stratospheric H_2O concentrations (for pressures less than ~100 hPa) are typically low, around 3-6 ppm (e.g. Wargan et al., 2023; Knowland et al., 2025). Compared to typical climatological values in the lowest troposphere, stratospheric water vapor amounts to about 0.05%, making its contribution to the total column measured by GOME-2 negligible. Typical GOME-2 averaging kernels for H_2O (and also for NO_2) are presented in the Supplement. Therefore, a correlation between QBO and total H_2O column is hardly expected in our results. On the other hand, correlations between total H_2O and natural oscillations in the troposphere such as ENSO and NAO are expected in our findings, as has been shown in previous studies (e.g. Trenberth et al., 2005; Trent et al., 2024). It should also be noted that the Hunga eruption in January 2022 injected a substantial amount of water vapor into the stratosphere affecting stratospheric circulation and climate (Yook et al., 2025). It was estimated that the stratospheric water vapor content went up by 10% while it may take several years for the H_2O plume to dissipate (Millán et al., 2022). The reason why GOME-2 may not "see" this impact is probably because its retrievals are insensitive to a 10% increase in stratospheric moisture.

3. Results and analysis

This section discusses the variability of total NO_2 and H_2O columns that is related to natural fluctuations such as the QBO, ENSO and NAO. The analysis is based on GOME-2A, 2B and 2C data and results are complemented with total H_2O data from CAMS reanalysis and total H_2O and NO_2 data from the RD1SD simulation with the EMAC CCM that cover a longer period (1979–2019). The annual cycle was removed from the datasets before examining the relations with the natural proxies as explained in section 2.

a. Quasi-Biennial Oscillation (QBO)

QBO dominates the variability of the equatorial stratosphere (16–50 km) and consists of downward propagating easterly and westerly wind regimes, with a variable period averaging approximately 28 months. Although it is a tropical phenomenon, it affects the

stratospheric flow from pole to pole by modulating the propagation and dissipation of the extratropical waves (Baldwin et al., 2001). There is also a secondary meridional circulation associated with the QBO, whereby the descending westerly phase induces anomalous downwelling over the equator, compensated by upwelling in the subtropics. The opposite is true for an easterly phase. This circulation affects temperature and atmospheric tracers in the lower stratosphere (Choi et al., 2002; Riberra et al., 2004). As the majority of the total NO_2 column is in the stratosphere, we have looked for a possible correlation between total NO_2 and the QBO. Figure 1 shows the correlation coefficients between the deseasonalized total NO_2 data from the GOME-2A and GOME-2B instruments and the equatorial zonal winds at 10 hPa. Blue colors show negative correlations and red colors show positive correlations with the zonal winds. The highest correlations are found in the tropics, as seen in all datasets, with positive correlations in the deep tropics and negative correlations in the subtropics. Although the GOME-2C data cover a much shorter period than the GOME-2A and 2B data, spanning nearly two QBO cycles, the correlations are in agreement with the other instruments (not shown). It is worth noting that results from GOME-2A are consistent with results from the EMAC RD1SD simulation for their common period 2007–2018 (Figure 1c). Also, the results from the GOME-2A and 2B data are consistent with the RD1SD model simulation results, which cover a longer period (1979–2019), as shown in Figure 1d.

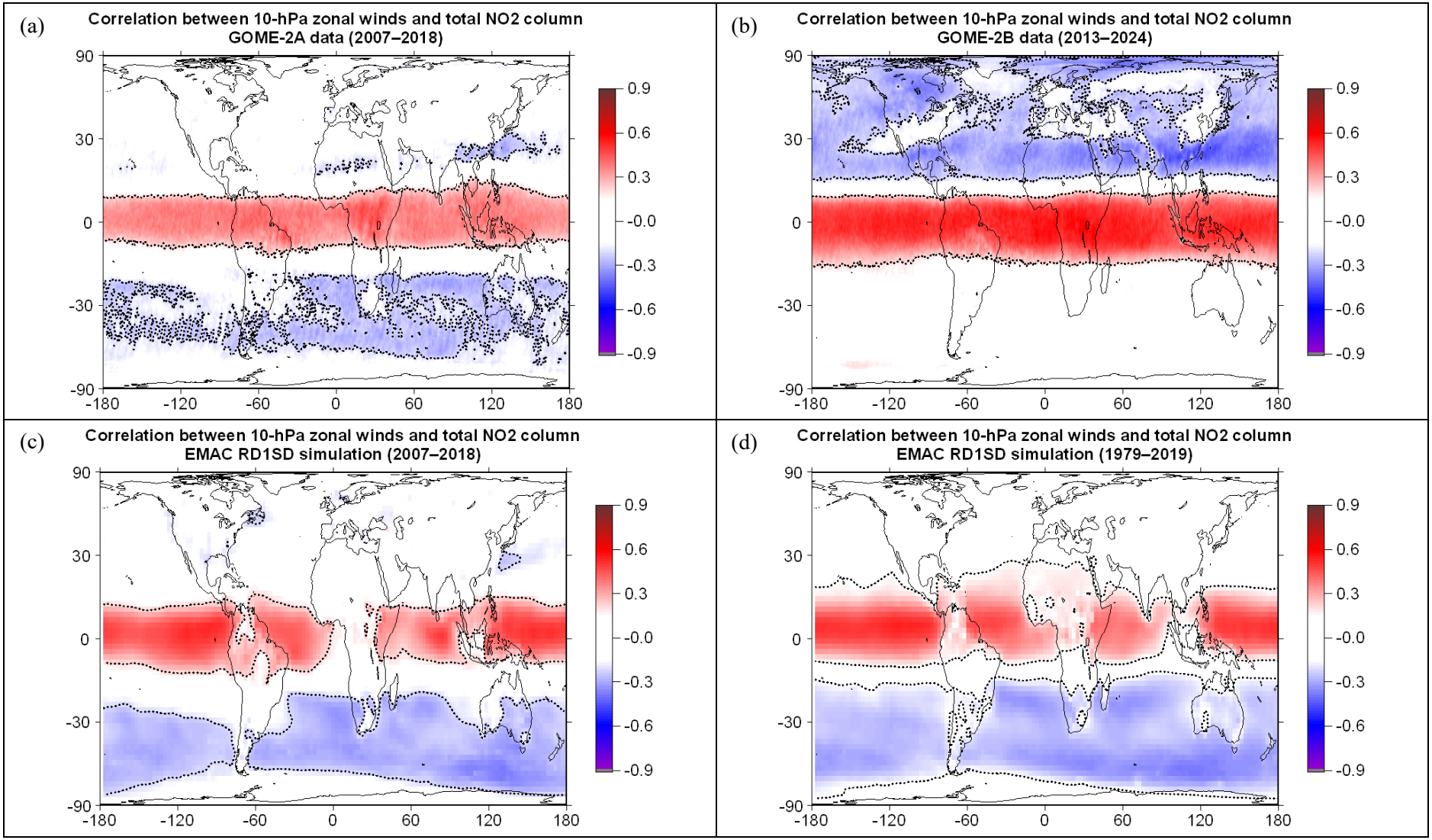

Fig. 1. Maps of correlation coefficients, *R*, between total NO_2 column anomalies and Singapore zonal winds at 10 hPa for (a) GOME-2A (2007-2018), (b) GOME-2B (2013-2024), (c) EMAC RD1SD simulation (2007-2018) (common period with GOME-2A) and (d) RD1SD model simulation results (1979-2019). Only *R* above/below ±0.15 are shown. Dotted lines bound regions where *R* are statistically significant at C.L. 99%. Anomalies were calculated after removing the seasonal cycle.

Figure 2 shows the respective correlation maps for the GOME-2A and 2B data but with equatorial zonal winds at 30 hPa. The results from the RD1SD model simulation are presented in Figures 2c and 2d, respectively. The correlations of total NO_2 with the zonal winds at 30 hPa change sign from what they were at 10 hPa due to the change in QBO phase from 10 to 30 hPa, and now become negative in the deep tropics and positive in the subtropics. In the deep tropics, the RD1SD model simulation results show weaker correlations than the GOME-2 data, but in the subtropics the model results agree quite well with the positive correlations revealed by the GOME-2 data, suggesting that the observed QBO-related variations in the total NO_2 column in the subtropics are well reproduced by the model simulation. We note here that the simulation was with "specified dynamics" (i.e., "nudged" by Newtonian relaxation towards ECMWF ERA-5 reanalysis data, and that also the zonal winds have been nudged in that setup. The weaker correlations in the deep tropics point to weak representation of the QBO in the lower stratosphere in the climate model simulation. However, it is outside the scope of this study to evaluate the different aspects of the model (dynamics, transport, evaporation, etc.), as this would require additional specific sensitivity simulations, which we have not done here. Our intention was just to analyze the simulation with specified dynamics nudged to ERA-5 reanalysis winds, in order to examine the full chemistry-climate scheme of the model simulation in terms of its ability to reproduce variability associated with natural oscillations.

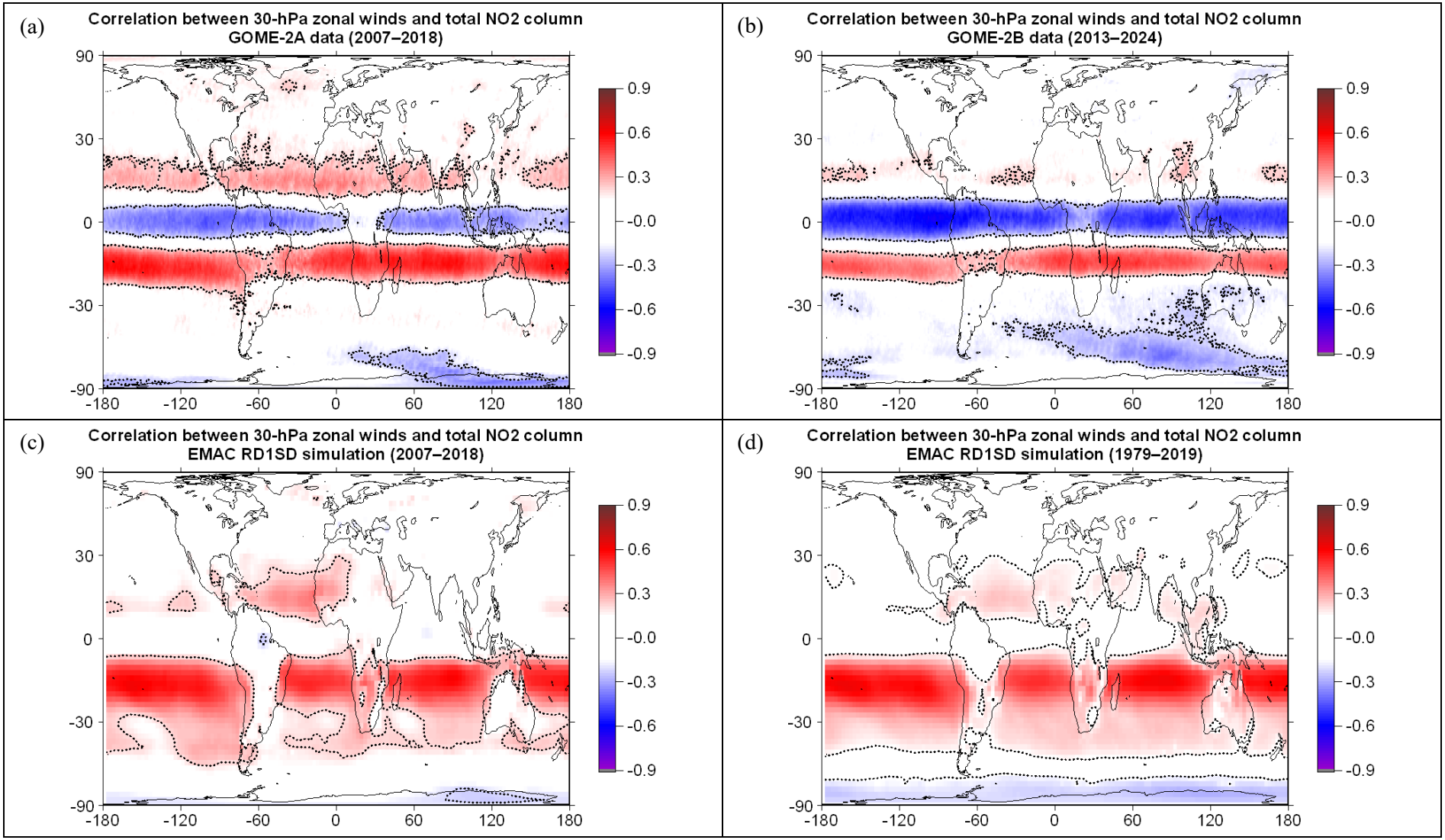

Fig. 2. Maps of correlation coefficients, *R*, between total NO_2 column anomalies and Singapore zonal winds at 30 hPa for (a) GOME-2A (2007-2018), (b) GOME-2B (2013-2024), (c) EMAC RD1SD simulation (2007-2018) (common period with GOME-2A) and (d) RD1SD model simulation results (1979-2019). Only *R* above/below ±0.15 are shown. Dotted lines bound regions where *R* are statistically significant at C.L. 99%. Anomalies were calculated after removing the seasonal cycle and correlations with 10 hPa zonal winds.

To have a better look at the variability of NO_2 associated with the QBO, Figure 3 shows the time series of total NO_2 anomalies and zonal winds at 30 hPa, after applying a 12-month running mean filter. The upper plot shows the northern subtropics (10°–30° N), the middle plot shows the deep tropics (10° N–10° S) and the lower plot shows the southern subtropics (10°–30° S). Red lines show GOME-2A data, blue lines show GOME-2B data, and green lines show GOME-2C data. The good agreement between the three instruments regarding the QBO fluctuation on total NO_2 is clearly seen. To corroborate the GOME-2 results, we have analyzed the respective results from the Ozone Monitoring Instrument (OMI) (lines with cyan color) from the dataset of Anglou et al. (2024). Yellow lines show the model simulation results. We also see the disruptions in the QBO cycle in the zonal wind data in 2015/2016 (e.g. Newman et al., 2016; Osprey et al., 2016; Coy et al., 2017) and 2019/2020 (e.g. Kang and Chun, 2021; Banyard et al., 2024), but a possible response of the total NO_2 column to these disruptions is not easy to determine from this figure. Tweedy et al. (2017) demonstrated a significant impact of the 2015/2016 disruption on ozone, including total ozone, so an influence on total NO_2 would be expected as well. To address the issue, we have compared the NO_2 anomalies during the disrupted QBO cycle of 2015/2016 with the composite of anomalies during the previous three undisrupted QBO cycles between 2007 and 2013. This composite was derived by a superposed epoch analysis, with zero lag placed at west wind maximum over the three QBO cycles before 2015, following the method by Zerefos et al. (1998). Zero lag was placed in June 2008, October 2010 and June 2013, respectively, when west wind at 30 hPa in Singapore was at its maximum value. We have extracted the deseasonalized anomalies of the three time series, starting 15 months before zero lag up to 30 months after zero lag, and then we calculated the average of the anomalies. This is the composite of NO_2 anomalies during the three QBO cycles prior to the disrupted QBO cycle of 2015/2016.

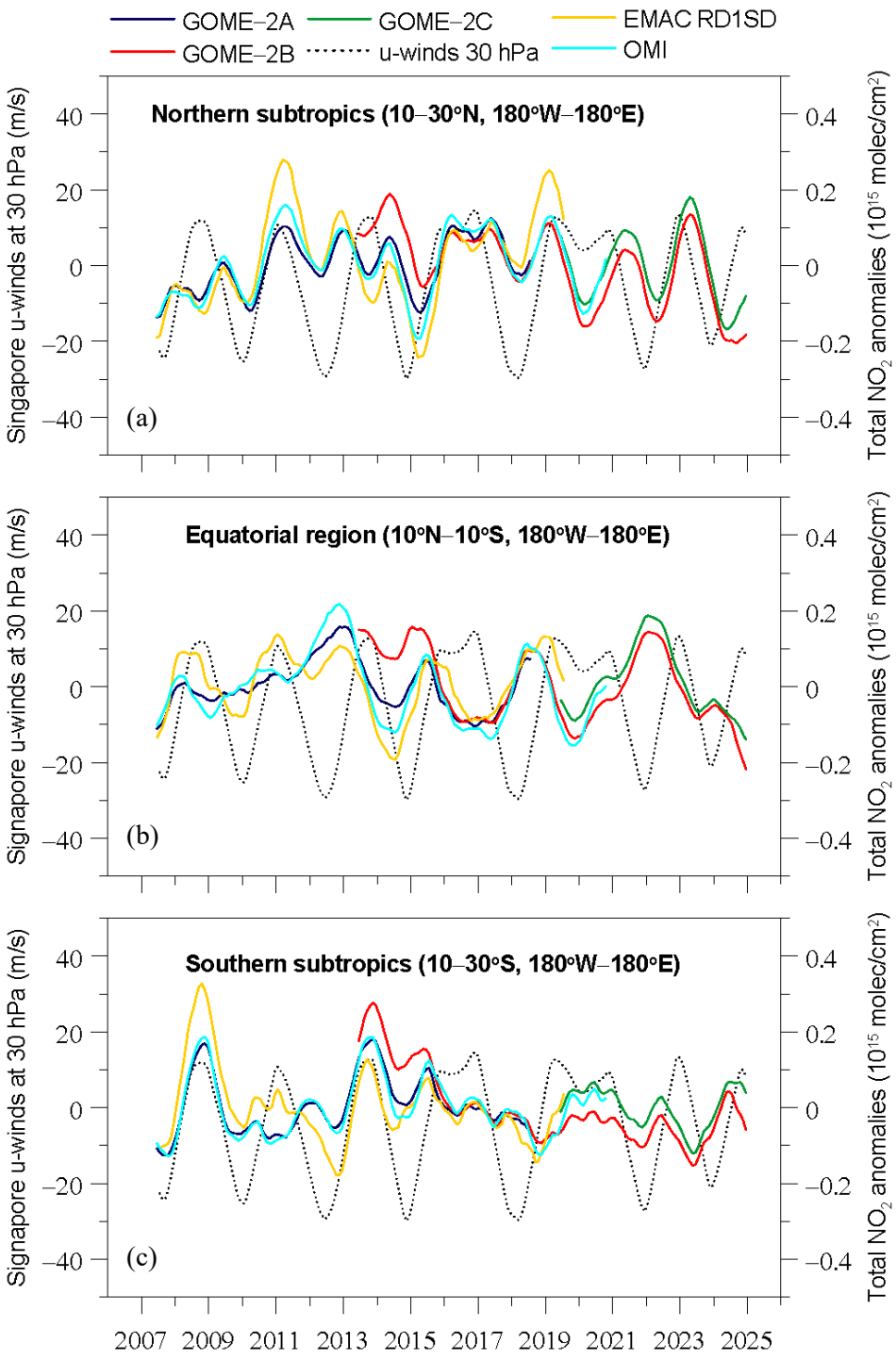

Fig. 3. Time series of total NO_2 anomalies and Singapore zonal winds at 30 hPa for (a) the northern subtropics (10°–30° N), (b) the equatorial region (10° N–10° S), and (c) the southern subtropics (10°–30° S). Anomalies were calculated after removing the seasonal cycle and a 12-month running mean filter has been applied.

The left panel of Figure 4 shows the composite of monthly mean zonal winds at 30 hPa in Singapore (panel a), in comparison to the composite of GOME-2A total NO_2 deseasonalized anomalies over 10^o N–10^o S (shown in panel b by the blue line), revealing the QBO effect on total NO_2 column in the tropics. The respective results from OMI from the dataset of Anglou et al. (2024) are shown by the orange line. The green line shows the deseasonalized NO_2 anomalies at the pressure level of 30 hPa from the EMAC RD1SD simulation. The middle panel of Figure 4 shows the 30 hPa zonal winds in Singapore during the disrupted QBO of 2015/2016, where the zero lag is placed in September 2015 (Figure 4c), and the response of total NO_2 from GOME-2A and OMI data to the disrupted QBO cycle (Figure 4d). Simulated NO_2 anomalies at 30 hPa are plotted as well. Finally, the right panel of Figure 4 shows the 30 hPa zonal winds in Singapore during the disrupted QBO cycle of 2019/2020 (Figure 4e) and the respective response of total NO_2 column from GOME-2B and OMI data (Figure 4f). Here, the zero lag was placed in March 2019.

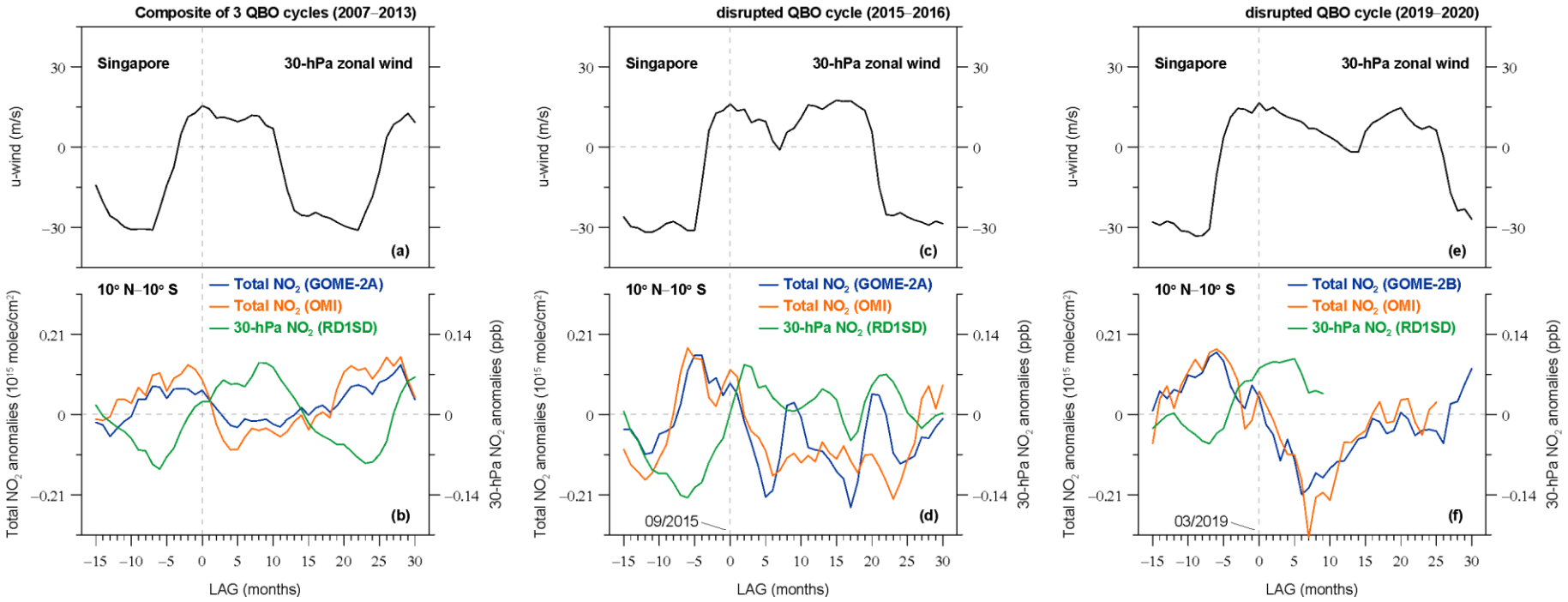

Fig. 4. Composite of three QBO cycles between 2007 and 2013 for (a) 30 hPa zonal wind in Singapore and (b) total NO_2 deseasonalized anomalies from GOME-2A and OMI data along with 30 hPa NO_2 deseasonalized anomalies from EMAC RD1SD simulation at 10° N – 10° S. (c) Zonal winds during the disrupted QBO cycle of 2015-2016 and (d) response of total NO_2 and 30 hPa NO_2 to the disrupted QBO cycle. (e) Zonal winds during the disrupted QBO cycle of 2019-2020 and (f) response of total NO_2 and 30 hPa NO_2 to the disrupted QBO cycle.

In general, it appears that the variation of total NO_2 from GOME-2A aligns well with the variation in total NO_2 from OMI (correlation coefficient = 0.885, $p < 0.0001$) and that fluctuations of total NO_2 column are out of phase with zonal winds at 30 hPa. Simulated NO_2 fluctuations at 30 hPa are very small, about 6 times smaller than at 10 hPa (not shown), and are in phase with the zonal winds at 30 hPa. From Figure 4b it appears that a westerly QBO phase at 30 hPa is mainly associated with negative anomalies of the NO_2 column and therefore decreased NO_2 amount, while an easterly QBO phase at 30 hPa is mainly associated with positive NO_2 column anomalies and therefore increased NO_2 amount. The QBO disruption during 2015/2016 and 2019/2020 is evident in zonal winds at 30 hPa where the normal descent of the easterly phase was interrupted by the persistent presence of westerly winds at 30 hPa. Comparing the variation in total NO_2 anomalies from Figure 4b (composite of undisrupted QBO cycles) with the variation in total NO_2 anomalies from Figures 4d and 4f (disrupted QBO cycles) we generally observe that total NO_2 anomalies remained negative for longer time periods than usual in response to the prolonged westerly winds at 30 hPa, resulting in reduced NO_2 amounts during periods with QBO disruption. Recent studies based on climate model simulations (e.g. Richter et al., 2020; Anstey et al. 2021; Wang et al., 2023) suggest that disruptions in the QBO cycle will occur more frequently in a warming climate, but the response of total NO_2 as well as of other trace gases to such disruptions is yet unknown.

The result of the distinct correlations of total NO_2 with the QBO is explained by the fact that the largest amount of nitrogen dioxide is found in the stratosphere, and in particular, about 80% of the total NO_2 column in the tropics lies in the stratosphere. As such, the stratospheric QBO is an important parameter affecting the natural variability of NO_2 in the tropics. Following Park et al. (2017), we have examined the vertical distribution of ozone versus NO_2 in the stratosphere and how that translates into the response to the QBO. To do so, we have unpacked the vertical structure of the response using the EMAC RD1SD simulation, similar to, Figs. 4 (ozone) and 5 (NOx) of Park et al. (2017). Our results refer to the period 2007–2018 (the GOME-2A period) and are presented in Figure 5 for the equatorial region 10° N–10° S. The upper and lower panels show the monthly mean deseasonalized NO_2 and ozone anomalies for the period 2007–2018, respectively. Monthly mean zonal winds from the ERA5 reanalysis are overlaid,

with solid lines indicating westerlies (W) and dotted lines indicating easterlies (E). It is known (e.g. Logan et al., 2003) that a descending westerly shear increases ozone below ~20 hPa (via subsidence) and decreases it above that level because of an increase in nitrogen oxides (NOx) which destroys ozone. This explains the negative O_3 anomalies and the corresponding positive NO_2 anomalies that we observe above ~20 hPa in Figure 5, in response to the westerly zonal winds (black solid lines). Below ~20 hPa, the results of the EMAC RD1SD simulation show increases in ozone in response to the QBO, consistent with Logan et al. (2003), but the response of NO_2 to the QBO is small. The smaller response of NO_2 to the QBO below 20 hPa is due to the dominant role of transport in that region rather than due to photochemical processes.

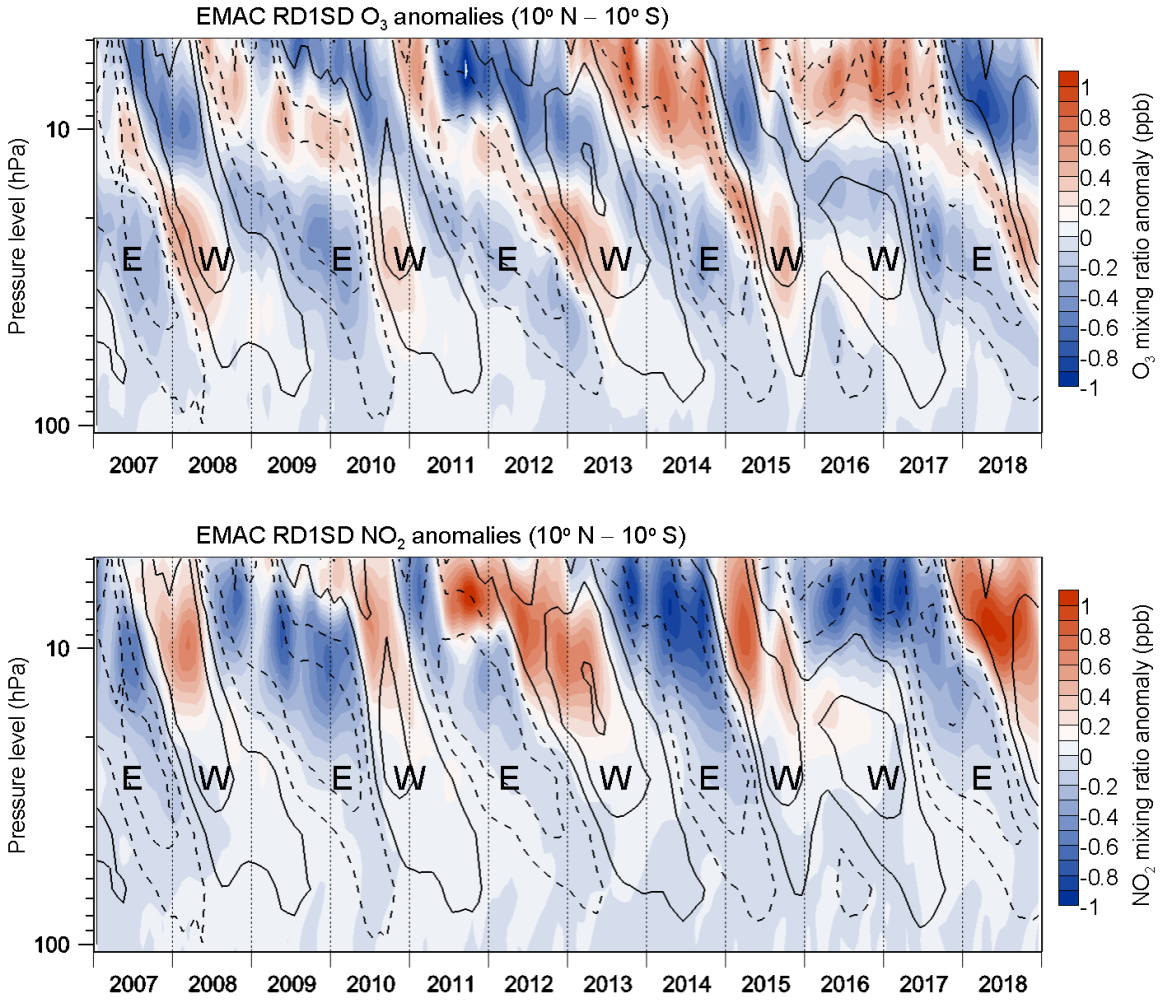

Fig. 5. Vertical structure of monthly mean deseasonalized O_3 (top) and NO_2 (bottom) anomalies from EMAC RD1SD simulation results for the period 2007-2018. Monthly averaged zonal mean winds from ERA-5 reanalysis data are overlaid as solid and dotted lines, representing westerly (W) and easterly (E) winds, respectively.

Our model results show that NO_2 anomalies propagate downward with the QBO, as was also shown by Park et al. (2017) for reactive nitrogen (NOy) species. Our results suggest that the partial NO_2 column that would be most appropriate to best reflect the influence of the QBO on total NO_2 variability is the one between 5 and 15 hPa. We have explored this further. To demonstrate the magnitude of the NO_2 fluctuations in response to the QBO, we present Figure 6 which shows the time series of deseasonalized NO_2 and O_3 anomalies from January 2007 to December 2018 in 10° N–10° S at various pressure levels, i.e. 5, 7, 10, 15, 20, 30, 50 and 70 hPa, relative to zonal (u) winds. *R* represents the correlation between NO_2 and O_3. The results show that NO_2 anomalies closely follow the variations of the zonal wind, and that NO_2 fluctuations are large between 5 and 15 hPa (within ±1 ppb for 5, 7, 10 hPa and within ±0.5 ppb for 15 hPa) and smaller at 20 hPa (within ±0.25 ppb). At 30 hPa the fluctuations of NO_2 relative to the QBO are even smaller (within ±0.125 ppb), while at 50 and 70 hPa they are too small (within ±0.075 ppb and ±0.05 ppb, respectively) compared to those above 15 hPa. We mention here that the correlation between NO_2 anomalies and zonal winds is positive. It is strong at 5, 7, 10, 15 and 20 hPa ($0.7<R<0.9$), moderate between 30 and 50 hPa ($0.5<R<0.6$) and weak at 70 hPa ($R<0.3$) (not shown). Combining all the above, we conclude that the parts of the NO_2 profile that contribute most to the response of the total NO_2 column to the QBO are those between 5 and 15 hPa. This explains the significant positive correlations between the simulated total NO_2 column anomalies and zonal winds at 10 hPa in the geographical region 10° N–10° S (shown in Figure 1) and is consistent with results from GOME-2 and OMI satellite data, which also give positive correlations between total NO_2 and 10 hPa zonal winds in the deep tropics. We remind that OMI satellite data were derived from the dataset of Anglou et al. (2024).

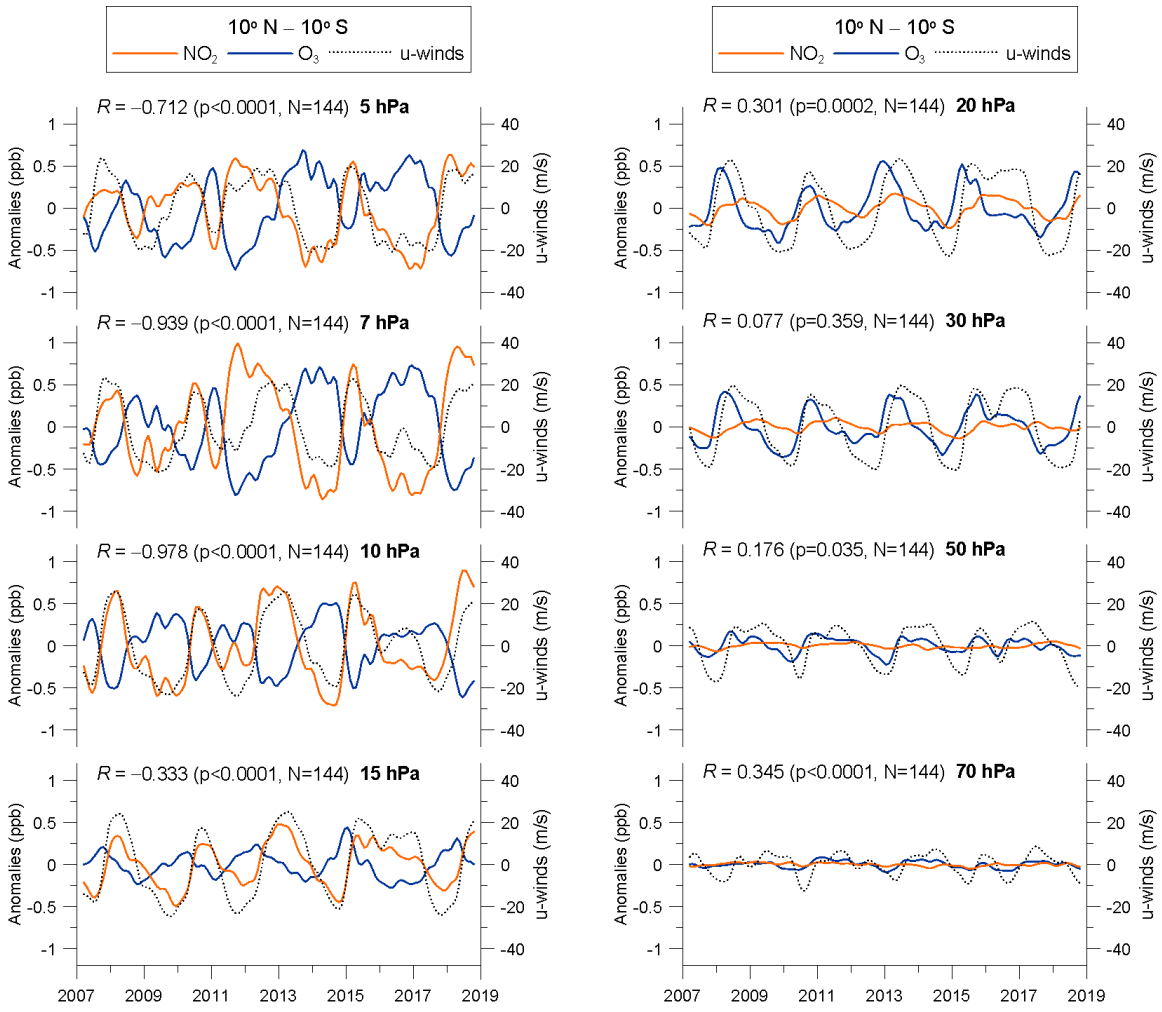

Fig. 6. Time series of deseasonalized NO_2 (blue) and O_3 (orange) anomalies at 5, 7, 10 and 15 hPa (left panel) and 20, 30, 50 and 70 hPa (right panel) in the tropics (10° N – 10° S) from 2007 to 2018, relative to zonal (u) winds. NO_2 and O_3 anomalies and u-winds are from the EMAC RD1SD model simulations. R is the correlation coefficient between NO_2 and O_3 anomalies.

At this point it is worth mentioning a few things about the correlations between O_3 and NO_2 from our simulations and how they compare with results from Park et al. (2017). We derive negative correlations between the two species above ~15 hPa, which agrees with results by Park et al., i.e. an anticorrelation between ozone and reactive nitrogen in the middle stratosphere above ~28 km (~15 hPa) due to NOx control of ozone catalytic cycles. More specifically, our anticorrelation between O_3 and NO_2 is mainly detected between 5 and 15 hPa, which agrees with results from Park et al., i.e. an anticorrelation of O_3 with NOx at altitudes of approximately 28–35 km. Park et al. (2017) find positive O_3–NOx correlation at 21 hPa, i.e. in the region where O_3 is under dynamical control, which is consistent with our result of positive O_3–NO_2 correlation at 20 hPa. Overall, Park et al. (2017) show strong positive correlations between O_3 and NOy (NOx+HNO_3) below ~28 km (~15 hPa) and negative correlations above, consistent with the change from dynamical control to photochemical control of O_3 across this level. We note here that our positive O_3–NO_2 correlations below ~15 hPa are small compared to the O_3–NOy correlations derived by Park et al., but this is likely explained by the NOy partitioning as a function of altitude, with HNO_3 dominating below ~15 hPa and NOx dominating above. In general, our estimates agree well with the results of Park et al., which supports the results of our model simulations.

Since the main QBO signal in the total NO_2 column at 10^o N–10^o S comes from heights between 5-15 hPa, it is not surprising that our model simulation does not yield significant correlations between total NO_2 and zonal winds at 30 hPa in this geographical region. This, however, is not in agreement with the GOME-2 satellite data, which show negative correlations between the total NO_2 column and 30 hPa zonal winds in the deep tropics. OMI supports the GOME-2 results. It is not clear why the model results do not show the observed negative correlations in the deep tropics, as indicated by the satellite data. Unfortunately, since GOME-2 only provides column measurements, we cannot examine the vertical distribution of NO_2 with the GOME-2 satellite data to see if it matches the model results or not. We note here that periods after major volcanic eruptions, which could have affected our correlation results, were not included in the regression analyses between zonal winds and simulated total NO_2 anomalies. More specifically, we have removed the periods 1982–1988 and 1991–1995 following Dubé et

al. (2020) to exclude the effects of the 1982 El Chichón, 1985 Nevado del Ruiz and 1991 Pinatubo volcanic eruptions. As such, we consider that our correlation estimates are not erroneously affected by large volcanic eruptions that could have masked the results of the simulated data. It should be mentioned, however, that the model simulation does not rule out the existence of negative correlations between total NO_2 and zonal winds at 30 hPa in the deep tropics. Calculations for shorter time periods, e.g. for the period 2013–2018, which is common between the model simulation and the GOME-2B satellite data, shows that the model simulation returns negative correlations between total NO_2 and zonal winds at 30 hPa in the deep tropics, which agree with those by GOME-2B, although they are smaller than them (see supplement Figure S2).

Our results also show a QBO signal in the NO_2 column in the extratropics, although it is less pronounced than in the tropics. Previous studies have shown that the QBO signal in NO_2 is not limited to the tropics but also extends to the extratropics (Zawodny and McCormick, 1991). This is a result of the QBO's influence on the meridional transport (north-south movement) of air masses in the tropical stratosphere, known as secondary meridional circulation, which transports nitrogen species from the tropics to higher latitudes, affecting the distribution and variability of NO_2. Analysis of SAGE II satellite data, such as in the work of Randel and Wu (1996), have documented the QBO signal in extratropical NO_2, showing that NO_2 anomalies in the extratropics are approximately out of phase with the tropical signal. Our results with the GOME-2 data show opposite correlations between the QBO and total NO_2 anomalies in the tropics and extratropics, in agreement with what has been documented in the previous studies. More specifically, Figure 1 indicates that the NO_2 QBO signal in the tropics is in phase with the equatorial zonal winds at 10 hPa, while the NO_2 QBO signal outside of the tropics is out of phase with them. In the tropics, positive NO_2 column anomalies (increased NO_2) are consistent with westerly zonal winds at 10 hPa, while negative NO_2 column anomalies (decreased NO_2) are consistent with easterly zonal winds at 10 hPa. On the other hand, outside of the tropics we observe negative NO_2 column anomalies during a westerly QBO phase at 10 hPa and positive NO_2 column anomalies during its easterly phase.

The opposite is observed if we compare the NO_2 column anomalies with the equatorial zonal winds at 30 hPa, which are in opposite phase to that at 10 hPa. Indeed, a

time lag is apparent between the 30 hPa winds and the NO_2 column response in the tropics. Therefore, the results in Figures 2 and 3 show negative and positive correlations between the NO_2 column anomalies and zonal winds at 30 hPa in the tropics and subtropics, respectively. We note here that the NO_2 column anomalies in the tropics are out of phase with the zonal winds at 30 hPa, while the NO_2 anomalies at the pressure level of 30 hPa are not. This, however, is not surprising, as the response of the total NO_2 column to the QBO is mainly dominated by the NO_2 response at 10 hPa rather than at 30 hPa, which is out of phase with the winds at 30 hPa. Figures 2 and 3 also suggest that the correlations are stronger in the Southern Hemisphere (SH) subtropics than in the Northern Hemisphere (NH) subtropics. This is consistent with previous findings based on Dutch OMI NO_2 (DOMINO) data, showing that the QBO effect on stratospheric NO_2 is more significant in the SH at 15^{o}S than in the NH (Dirksen et al., 2011, Figure 15). The DOMINO data also showed a clear interhemispheric asymmetry in the NO_2 QBO with its peak value being nearly 2 times larger in the SH than in the NH (Dirksen et al., 2011).

Past research (e.g. Kinnersley and Tung, 1998) has shown that the QBO signal for trace gases like ozone is stronger in the SH extratropics than in the NH, attributed to differences in stratospheric dynamics and wave forcing, with a clearer correlation with the equatorial QBO in the SH. In the NH, by contrast, the observed high-latitude ozone anomaly was not well correlated with the equatorial QBO (Kinnersley and Tung, 1998). The NH's extratropical response to the QBO is significantly influenced by the inter-annual variability of planetary wave forcing, which is larger in the NH than in the SH. The greater influence of stratospheric planetary waves in the NH may lead to a weaker and more variable QBO signal in that hemisphere for chemical tracers like NO_2, making the signal more apparent in the SH. Therefore, the observation that the QBO signal is more pronounced in the SH extratropics for NO_2 is supported by studies showing a stronger QBO amplitude and clearer statistical correlations between SH circulation and the QBO compared to the NH. This probably explains why in Figure 1 we derive stronger correlations between equatorial zonal winds and extratropical total NO_2 anomalies in the SH than in the NH with GOME-2A data and EMAC RD1SD simulation results. This, however, may not always be the case, as there may be periods that exhibit stronger correlations with the QBO in the NH extratropics, leading to more pronounced QBO-

related NO_2 column anomalies, while other periods may exhibit weaker correlations. For example, the GOME-2B data show strong correlations with the QBO in the NH during the period 2013–2024 and therefore the signal of QBO in NH extratropical NO_2 column variability is clearly visible in this period. However, it is not as visible in the period 2007–2018 according to GOME-2A data and RD1SD simulation results. Results from GOME-2C data agree well with those from GOME-2B (not shown). We note here that the examination of the correlations for the period 2013–2018, which is common between GOME-2A, GOME-2B, OMI satellite data and EMAC RD1SD simulation, returns similar correlation results in the extratropical NH regions (see supplement Figure S3), which corroborates the agreement between the different datasets.

Anstey et al. (2022) pointed out that many climate models are now able to simulate QBO-like oscillations, but with systematic errors, such as a too weak amplitude in the lower stratosphere, and that improving the representation of the QBO in models is difficult due to uncertainties in observations and in understanding of the waves that drive this oscillation. Considering these remarks, we believe that the ability of newer versions of the GOME-2 instrument to correctly capture QBO-related variations in chemical species, such as columnar NO_2, may significantly assist in evaluating the representation of the QBO in climate model simulations in the coming years.

We also examined the correlation between the stratospheric QBO and the total H_2O column, but there were no significant results (correlation coefficients between the two parameters are less than 0.3). This is not surprising given that in practice GOME-2 mainly measures the tropospheric H_2O column, as explained in Section 2. As such, a correlation between QBO and (in practice tropospheric) GOME-2 H_2O column can hardly be expected in our results. Therefore, maps showing the correlation coefficients between the two parameters or plots showing the time series of data anomalies along with QBO are not presented for the total H_2O column. The next section analyses the effect of El Niño Southern Oscillation (ENSO), which shows a clear impact on the total H_2O column. This is also not surprising, since ENSO is a large-scale phenomenon in the troposphere where almost all of H_2O is located.

b. El Niño Southern Oscillation (ENSO)

ENSO is the term used to describe the oscillation between El Niño and La Niña events. The term El Niño refers to the extensive warming of the central and eastern tropical Pacific Ocean that leads to a major shift in weather patterns across the Pacific. This occurs every three to eight years and is associated with a weaker Walker Circulation. La Niña is the opposite of an El Niño event and is associated with the cooling of the central and eastern tropical Pacific. ENSO has a profound influence on global climate, weather and ecosystems. Determining how the ENSO responds to greenhouse warming is a crucial issue in climate science (Hu et al., 2021). ENSO is coupled with ocean heat storage thereby influencing terrestrial energy budget (Hogikyan et al. 2022) through clouds (Ceppi and Fueglistaler, 2021) and surface solar radiation (Chtirkova et al., 2023). ENSO has long been known to affect the atmospheric circulation at the earth's surface all over the world, its signal to appear both in the middle troposphere and in the stratosphere of the Northern Hemisphere (van Loon et al., 1982), and, also to affect the variability of important atmospheric gases such as total ozone (Zerefos et al., 1982). Eleftheratos et al. (2019) presented correlations between total ozone and ENSO using GOME-2A data, and the results showed statistically significant correlations mainly in the tropics. Olsen et al. (2016) found impacts of ENSO on extratropical tropospheric column ozone. Here, we examine the correlation between ENSO and total columns of H_2O and NO_2 from GOME-2 data.

Figure 7 shows correlation maps between total H_2O anomalies from GOME-2A, GOME-2B measurements and the Niño3.4 index. Anomalies were derived after subtracting the seasonal cycle and variability associated with the QBO from Equations (1) and (2). The upper panel shows the correlation coefficients between (a) GOME-2A and Niño3.4 index and (b) GOME-2B and Niño3.4 index, and the lower panel shows the correlation coefficients between (c) CAMS reanalysis and Niño3.4 index and (d) EMAC RD1SD simulation and Niño3.4 index. GOME-2A and GOME-2B maps show consistent similarities with each other and CAMS reanalysis shows excellent agreement with the GOME-2 data. Figure 7d, which shows the respective correlation map between Niño3.4 index and RD1SD model simulation results, refers to the longer period 1979–2019. From Figure 7 it appears that the agreement in spatial correlation patterns between the various

maps is quite high, despite the different time periods studied. The close similarity between these correlation maps provide evidence that all data sets (GOME-2A, GOME-2B, CAMS reanalysis and EMAC RD1SD simulation) realistically reproduce the response of total column H_2O to ENSO.

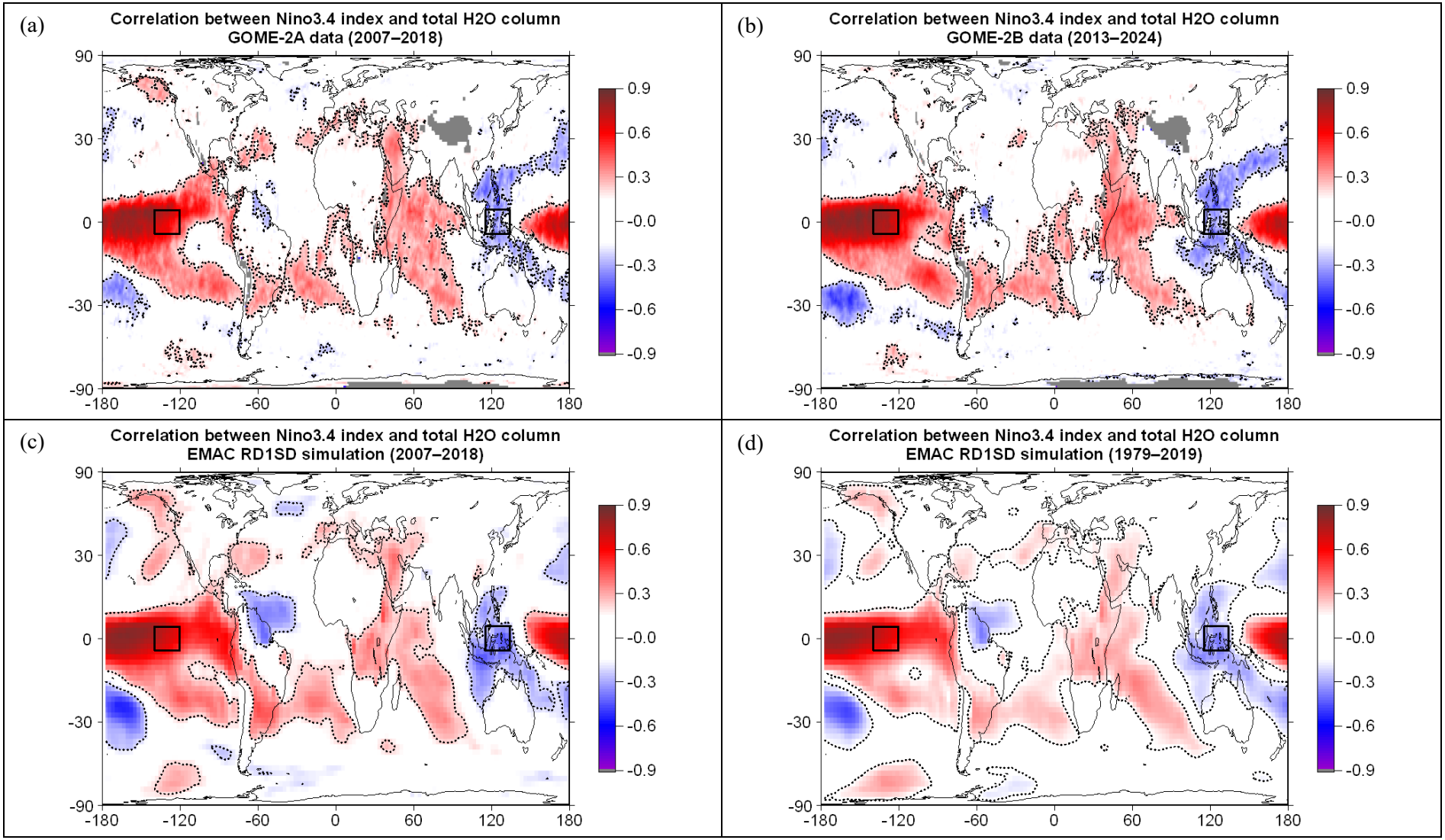

Fig. 7. Maps of correlation coefficients, *R*, between total H_2O column anomalies and Niño3.4 index for (a) GOME-2A (2007–2018), (b) GOME-2B (2013–2023), (c) CAMS reanalysis (2003–2024) and (d) EMAC RD1SD simulation results (1979–2019). Only *R* above/below ±0.15 are shown. Dotted lines bound regions where *R* are statistically significant at C.L. 99%. Anomalies were calculated after removing the seasonal cycle and variability related to the QBO.

More specifically, all maps show a strong dipole of opposite correlation coefficients between the eastern and western tropical Pacific Ocean. The correlations were performed for month lag 0. Analysis of correlations for different time lags was not performed. The total H_2O column is positively correlated with Niño3.4 index over the eastern part of the tropical Pacific Ocean and negatively correlated over its western part. To investigate the variability of total H_2O during ENSO events, Figure 8 shows the time series of H_2O column anomalies for two regions in the tropical Pacific Ocean, one region in the eastern tropical Pacific bounded by latitudes 5º N–5º S and longitudes 120º–140º W, and one region in its western part bounded by latitudes 5º N–5º S and longitudes 115º–135º E. The anomalies were obtained after removing the seasonal cycle and QBO variability from Equations (1) and (2). The blue, red, and green lines show GOME-2A, GOME-2B, and GOME-2C data, respectively, and the deep yellow line shows CAMS data. The dotted line shows the ENSO index (Niño3.4 index). The line with cyan color show results from the EMAC RD1SD simulation. The graphs show that in the region in the eastern tropical Pacific Ocean there is a positive correlation with the Niño3.4 index, while in the region in the western tropical Pacific Ocean there is a negative correlation with the Niño3.4 index.

In both regions, GOME-2A, GOME-2B and GOME-2C data are strongly correlated with each other and the CAMS reanalysis data show excellent agreement with the GOME-2A, 2B and 2C data. In the eastern Tropical Pacific Ocean (Figure 8a), the H_2O column increases during warm (El Niño) events and decreases during cold (La Niña) events. Our correlation patterns in the tropical Pacific Ocean are consistent with the regression patterns of precipitable water with ENSO as presented by Trenberth et al. (2005), who showed positive regressions in the central/eastern Pacific and negative regressions in its western part. Trenberth et al. focused, however, on trends in column-integrated atmospheric water vapor which we do not analyze here. Our results also agree with results previously shown by Eleftheratos et al. (2007), who linked the observed increases in cirrus cloud cover to increased rising of warm moist air over the eastern tropical Pacific during El Niño, and thereby enhanced convective activity in the area. The opposite behavior is observed in the western part of the tropical Pacific Ocean (Figure 8b), which shows a positive correlation between the H_2O column and Niño3.4 index. In this part of the Pacific, reduced convection in the area is associated with reduced amounts

of H_2O during El Niño events. Our results for the eastern Pacific are also in agreement with Lelli et al. (2014) who investigated changes in cloud top height and cloud fraction for low, middle and high clouds in relation to ENSO over the central East Pacific. Their results for the east-central equatorial Pacific (170–120° W, 5° N–5° S) showed that during positive ENSO phases, positive SST anomalies promote greater evaporation, thereby increasing cloud cover near the surface. At the same time, the related enhancement in convection (i.e. positive anomalies in cloud altitude anomalies) are related to weaker trade winds and enhanced meridional convergence of air masses, leading to both a decrease in cloudiness in the mid troposphere and an increase closer to the tropopause.

In the period 2007–2024 there were two major El Niño and two major La Niña events. The major El Niño events were recorded in 2015–2016 and 2023–2024 and the major La Niña events were recorded in 2010–2012 and 2020–2023. The increase of total H_2O in the eastern Tropical Pacific region during these two major El Niño events is evident in all examined datasets (Figure 8a). During April 2015 – March 2016 the increase reached or exceeded 10 kg/m^2, depending on the dataset, which corresponds to about 25% of the regional mean, with the regional mean being about 40 kg/m^2. Accordingly, in the other part of the Tropical Pacific region, the decrease in H_2O column reached or exceeded 7.5 kg/m^2 or 14% of the mean, with the mean being about 52 kg/m^2 (Figure 8b). Observed fluctuations in H_2O column during La Niña episodes are also consistent between the different datasets. Such kind of analyses help us to understand the magnitude of the H_2O column changes during strong ENSO events of the recent past. Changes of total H_2O by the CAMS reanalysis (deep yellow line) are in full agreement with the GOME-2 satellite data. It also appears that the EMAC CCM simulates well the variability of total H_2O related to ENSO. The magnitude of the simulated H_2O column anomalies is consistent with the GOME-2 and CAMS data, and the results of the correlation analyses match well those of satellite GOME-2 and CAMS reanalysis data, as shown in Table 1. The time series of Niño3.4 index and total H_2O anomalies from the RD1SD model simulation for the long-term period 1979–2019 can be found in the supplement Figure S4.

It should be mentioned here that the statistical comparisons presented in Table 1 for ENSO (and later in Table 2 for NAO) demonstrate a strong agreement among the various datasets in capturing ENSO (and NAO) signals. As shown in these tables, all slopes are positive, resulting in positive correlation coefficients; however, the slope values differ from unity, being either greater or lower than one. In general, a slope between two variables (X, Y) that is less than one indicates that as X increases, Y also increases, but to a lesser extent, implying that the covariance of X and Y is smaller than the variance of X. Conversely, a slope greater than one indicates that as X increases, Y increases more strongly, implying that the covariance of X and Y exceeds the variance of X. This information could be valuable for researchers seeking to extend, for example, the GOME-2A time series to the present using regression coefficients (intercept and slope) derived from comparisons with GOME-2B or CAMS data—an application that lies beyond the scope of the present study. For convenience, we provide here the mathematical formulas of the slope, covariance and variance. The slope is given from the covariance of two variables (X,Y) divided by the variance of variable X, i.e.,

$$slope = \frac{covariance(X,Y)}{variance(X)}$$

The covariance(X,Y) is calculated with the formula:

$$covariance(X,Y) = \frac{\sum_{i=1}^{N}(X_i - \bar{X})(Y_i - \bar{Y})}{N-1}$$

Where, N is the number of pairs, $\bar{X}$ is the mean of X, and $\bar{Y}$ is the mean of Y. And the variance(X) is defined by the following formula:

$$variance(X) = \frac{\sum_{i=1}^{N}(X_i - \bar{X})^2}{N-1}$$

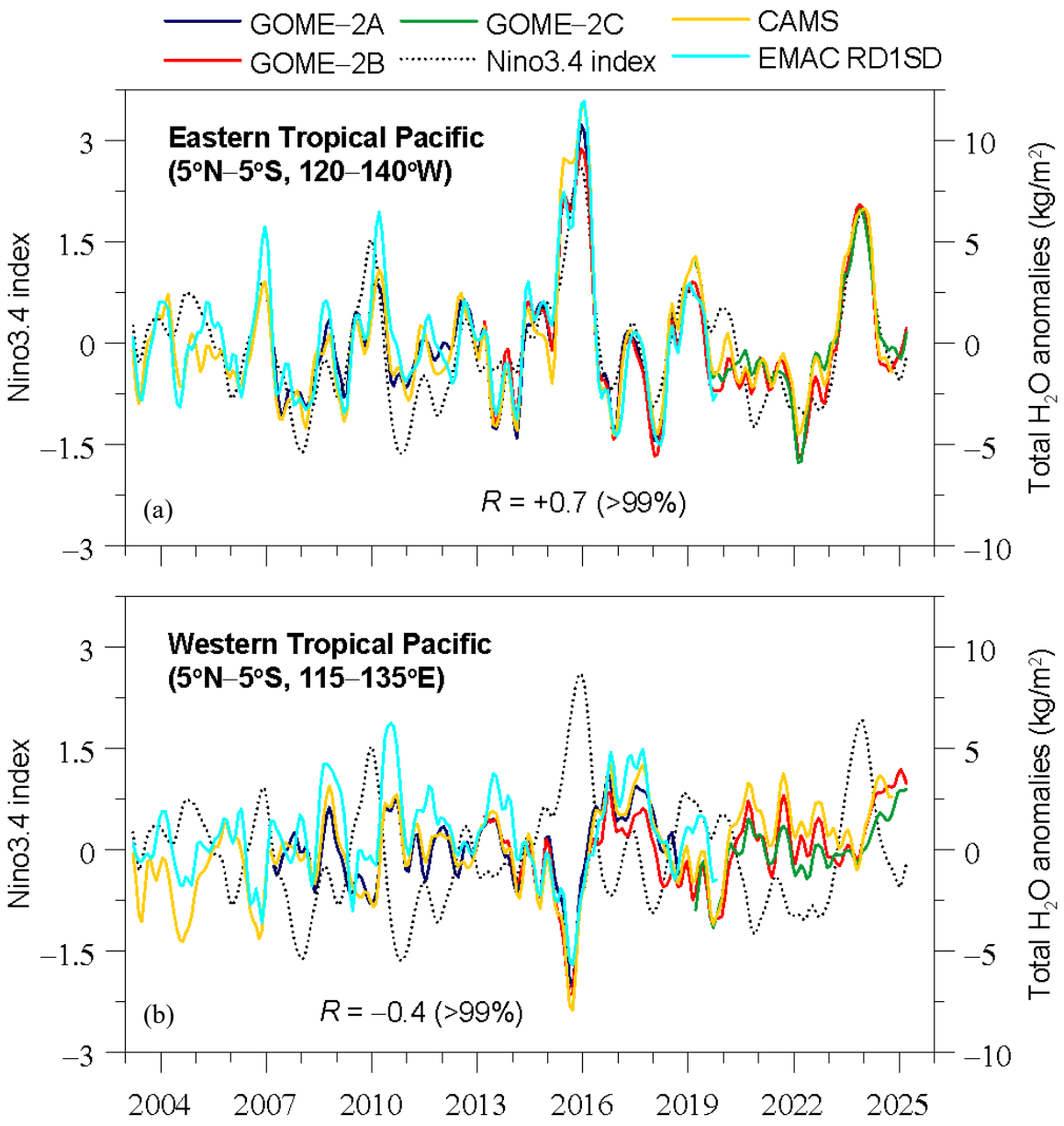

Fig. 8. Time series of total H_2O column anomalies from GOME-2A, GOME-2B, GOME-2C data, CAMS reanalysis, and EMAC RD1SD simulation results compared to Niño3.4 index for two regions in the Tropical Pacific Ocean (a) eastern Tropical Pacific (5° N–5° S, 120°–140° W) and (b) western Tropical Pacific (5° N–5° S, 115°–135° E). Anomalies were calculated after removing the seasonal cycle and variability related to the QBO. *R* is the correlation coefficient between CAMS data and Niño3.4 index. Values in parentheses refer to statistical significance of *R*. A low-pass filter with weights 1-4-6-4-1 has been applied to the H_2O column anomalies and the Niño3.4 index. The low-pass filter

was applied for visualization purposes and not in the correlation analysis. All correlation calculations were conducted using the monthly anomaly data without any low-pass filtering.

(a) Eastern Tropical Pacific region (5º N–5º S, 120º–140º W)						
	Correlation	Slope*	Error	*t*-value	*p*-value	*N*
GOME-2A vs GOME-2B	0.982	1.018	0.024	42.986	<0.0001	72
GOME-2A vs CAMS	0.963	0.863	0.020	42.403	<0.0001	144
GOME-2A vs RD1SD	0.888	0.809	0.035	23.043	<0.0001	144
GOME-2B vs GOME-2C	0.960	1.015	0.034	29.626	<0.0001	77
GOME-2B vs CAMS	0.963	0.891	0.021	43.335	<0.0001	149
GOME-2B vs RD1SD	0.912	0.835	0.042	20.077	<0.0001	84
GOME-2C vs CAMS	0.936	0.903	0.039	22.957	<0.0001	77
CAMS vs RD1SD	0.858	0.857	0.036	23.706	<0.0001	204
(b) Western Tropical Pacific region (5º N–5º S, 115º–135º E)						
GOME-2A vs GOME-2B	0.933	0.959	0.044	21.658	<0.0001	72
GOME-2A vs CAMS	0.909	0.817	0.031	25.949	<0.0001	144
GOME-2A vs RD1SD	0.689	0.555	0.049	11.320	<0.0001	144
GOME-2B vs GOME-2C	0.904	1.076	0.059	18.323	<0.0001	77
GOME-2B vs CAMS	0.918	0.836	0.030	28.140	<0.0001	149
GOME-2B vs RD1SD	0.776	0.696	0.063	11.139	<0.0001	84
GOME-2C vs CAMS	0.879	0.752	0.047	15.996	<0.0001	77
CAMS vs RD1SD	0.777	0.728	0.042	17.543	<0.0001	204

*Error, *t*-value, *p*-value refer to slope.

Table 1. Statistics of correlations between monthly total H_2O anomalies from GOME-2A, GOME-2B, GOME-2C, CAMS reanalysis and EMAC RD1SD simulation results for their common periods, over two regions affected by ENSO, (a) the eastern Tropical Pacific region (5º N–5º S, 120º–140º W) and (b) the western Tropical Pacific region (5º N–5º S, 115º–135º E). Anomalies were calculated after removing the seasonal cycle and variability related to the QBO.

Comparing our results with those by Trent et al. (2024), we observe that the pattern of correlations between ERA5 total column water vapor and ENSO shown in Figure 12 of Trent et al. is consistent with the pattern of correlations presented in our study, providing strong evidence that the GOME-2 data perform well in capturing the variability in total column water vapor associated with ENSO. But why is it important to know whether the GOME-2 instruments depict well the H_2O variability associated with ENSO events? Cai et al. (2014) presented evidence, based on climate modelling, for a doubling of the occurrence of extreme El Niño events in the future in response to greenhouse warming. Cai et al. (2023) linked the more frequent strong El Niño and La Niña events after 1960 to anthropogenic warming. More recently, Lu et al. (2025) showed that over the past 7000 years, the ratio of multi-year to single-year ENSO events increased by a factor of 5, associated with a longer ENSO period (from 3.5 to 4.1 years). In view of these results, high-quality measurements are the best tool we can have to improve our knowledge of the response of climate variables to past and recent ENSO episodes, to examine the reliability of climate model simulations, and to assess with greater certainty the risks associated with extreme ENSO events. In this regard, the agreement we find between the GOME-2A and GOME-2B H_2O anomalies during the major El Niño event of 2014-16 and between the GOME-2B and GOME-2C H_2O anomalies during the recent major El Niño event of 2023-24 indicates that the use of data from the newer GOME-2 instruments can be quite reliable for quantifying changes in water vapor during upcoming El Niño events. Good agreement is also observed during the strong La Niña event of 2010-12 and the prolonged La Niña event of 2020-23. Therefore, we strongly believe that the GOME-2 measurements of total column water vapor can be quite useful to qualitatively and quantitatively assess the performance of climate model simulations during El Niño and La Niña events in future water vapor assessments.

Finally, we note that we performed the same analysis of correlations between ENSO and the total NO_2 column. We find statistically significant correlations between ENSO and total NO_2 anomalies in tropical regions after removing seasonal and QBO-related variations, the majority of which is within ±0.4. The results are presented in Figure 9, which shows the estimated correlation coefficients between ENSO and total NO_2 column from GOME-2A (2007–2018) and GOME-2B (2013–2024) measurements, together with

RD1SD model simulation results for the same period with GOME-2A (2007–2018) and for the long-term period 1979–2019.

Positive correlation coefficients are found over Southeast Asia and Indonesia and negative ones over the central and eastern parts of the tropical Pacific Ocean. Positive correlations are shown in red and indicate positive NO_2 column anomalies during El Niño events, while negative correlations are shown in blue and indicate negative NO_2 column anomalies, respectively. Inness et al. (2015) estimated NOx anomalies at 500 hPa from the Monitoring Atmospheric Composition and Climate (MACC) reanalysis by subtracting the La Niña composite (2005, 2007, 2008, 2010, 2011) from the El Niño composite (2004, 2006, 2009). They identified negative anomalies over the eastern Pacific that coincided with reduced O_3 levels, suggesting enhanced upward transport of NOx-poor air to these altitudes. The negative NO_2 column anomalies that we observe over the central and eastern Pacific during El Niño may be linked to the same processes. Thus, the NO_2 column decreases in the central and eastern Pacific. On the other hand, the amount of NO_2 increases over the Indonesian area and therefore the correlation between ENSO (Niño3.4 index) and the NO_2 column is positive. This is explained by the fact that El Niño events cause abnormally dry conditions in the Western Pacific, which often cause a dramatic increase of areas affected by biomass burning. The latter emits large amounts of ozone precursors into the troposphere, such as nitrogen oxides, carbon monoxide and hydrocarbons, affecting the composition of the atmosphere (e.g. Loyola et al., 2006), and therefore the NO_2 column increases. The model results are generally in agreement with GOME-2 results in terms of correlations over the tropical Pacific Ocean, but the signals in the model results are more pronounced than in the GOME-2 data. We note here that with the model we separated the tropospheric from the total NO_2 column and calculated the correlation coefficients between tropospheric NO_2 anomalies and ENSO (Figure S5). The overall correlation patterns in the tropical Pacific Ocean is nearly identical for both the total and tropospheric NO_2 columns; however, correlations with ENSO in the tropical Pacific are stronger for the tropospheric data than for the total NO_2 data. This indicates that it is primarily the tropospheric NO_2 column that is affected by ENSO-related variability.

Examples of the magnitude of fluctuations in total NO_2 anomalies in relation to ENSO are presented in Figure 10 for two selected regions, one over the central tropical Pacific Ocean (5° N–5° S, 160°–180° W) and one over the Indonesian area (0°–10° S, 100°–120° E). Previous studies have shown that the 2015 Indonesian fire season, in terms of fire activity and pollution, was the most severe since NASA's Earth Observing satellite system began observations in the early 2000s (Field et al., 2016), and that carbon emissions from fires over maritime southeast Asia associated with the 2015 El Niño were larger than those associated with the record-breaking 1997 El Niño (Huijnen et al., 2016). Our results with GOME-2A data, which had measurements available during the strong El Niño event in 2015/2016, show that the column NO_2 increased in the Indonesian region in 2015/2016 by up to 0.27 x 10^{15} molecules/cm^2 (or 17.1% of the mean) with the mean being 1.58 x 10^{15} molecules/cm^2, and decreased in the central tropical Pacific region by up to 0.24 x 10^{15} molecules/cm^2 (or 17.8% of the mean) with the mean being 1.35 x 10^{15} molecules/cm^2. Similar fluctuations in NO_2 column anomalies during 2015/2016 are also estimated from the GOME-2B data and the EMAC RD1SD simulation, respectively.

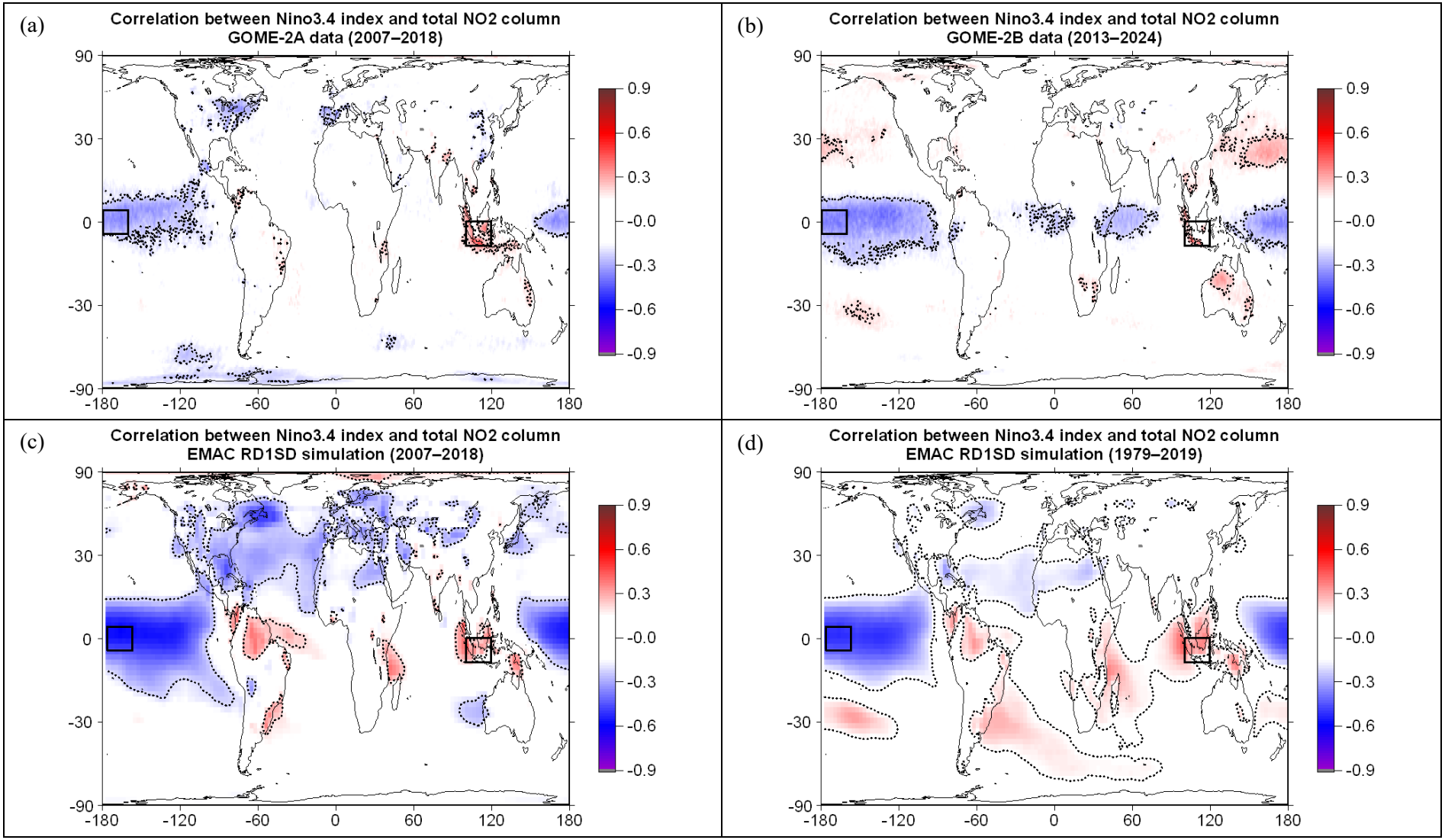

Fig. 9. Maps of correlation coefficients, R, between total NO_2 column anomalies and Niño3.4 index for (a) GOME-2A (2007–2018), (b) GOME-2B (2013–2023), (c) EMAC RD1SD simulation (2007–2018) and (d) EMAC RD1SD simulation results (1979–2019). Only R above/below ±0.15 are shown. Dotted lines bound regions where R are statistically significant at C.L. 99%. Anomalies were calculated after removing the seasonal cycle and variability related to the QBO.

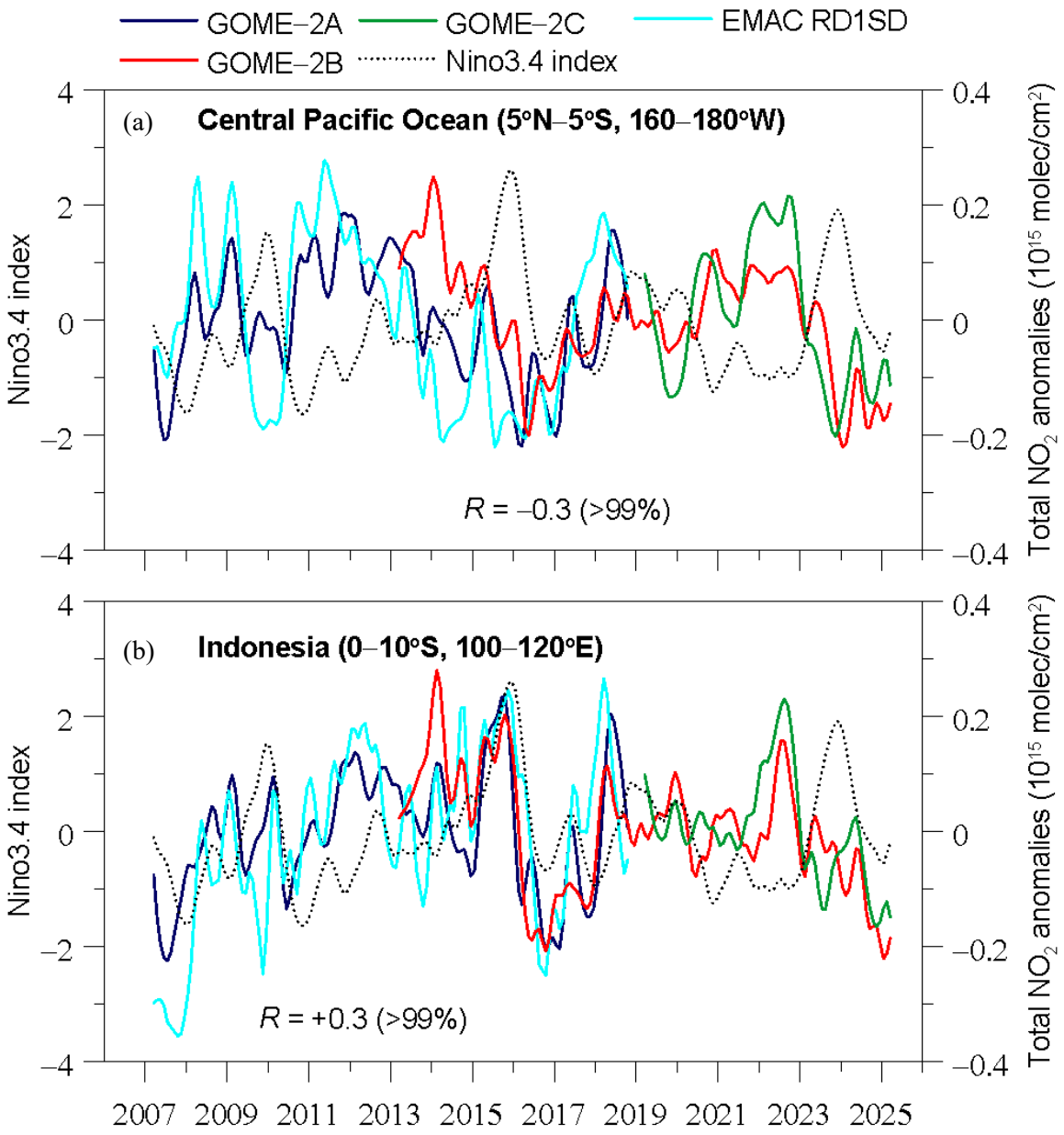

Fig. 10. Time series of total NO_2 column anomalies from GOME-2A, GOME-2B, GOME-2C data and EMAC RD1SD simulation results compared to Niño3.4 index for two regions (a) Central Pacific Ocean (5° N–5° S, 160°–180° W) and (b) Indonesia (0°–10° S, 100°–120° E). Anomalies were calculated after removing the seasonal cycle and variability related to the QBO. *R* is the correlation coefficient between GOME-2A data and Niño3.4 index. Values in parentheses refer to statistical significance of *R*. A low-pass filter with weights 1-4-6-4-1 has been applied to the NO_2 column anomalies and the Niño3.4 index. The low-pass filter was applied for visualization purposes and not in the

correlation analysis. All correlation calculations were conducted using the monthly anomaly data without any low-pass filtering.

c. North Atlantic Oscillation (NAO)

Next, we analysed the effects of NAO on the examined trace gases. NAO is one of the most prominent and recurrent patterns of atmospheric circulation variability. It affects climate variability from the eastern seaboard of the United States to Siberia and from the Arctic to the subtropical Atlantic, especially during boreal winter, so variations in the NAO are important to society and for the environment (Hurrell et al., 2003). Understanding the implications of NAO on atmospheric parameters is important in the context of global climate change.

Figure 11 shows maps of correlation coefficients between the NAO index and the total H_2O column anomalies from (a) GOME-2A (2007-2018), (b) GOME-2B (2023-2024), (c) CAMS reanalysis (2003-2024), and (d) EMAC RD1SD simulation (1979–2019). Anomalies were computed after removal of the seasonal cycle and variability associated with the QBO and ENSO from Equations (1), (2), and (3). As can be seen from Figure 11, there are consistent similarities in the pattern of correlation coefficients between the GOME-2A, GOME-2B datasets and the NAO index in the northern extra tropics, which is interesting.

Blue colors show negative correlations and red colors show positive correlations with the NAO index. Positive correlations are observed along a path that begins from the Caribbean Sea, crosses the North Atlantic Ocean on a northerly track towards Europe, and extends along Northeast Asia. Northwest of this path in the North Atlantic we observe a wide region of negative correlations south of Greenland and in Northeast Canada. Negative correlations are also observed southeast of this path over the southern North Atlantic, west of the coast of Northwest Africa. These results are based on the GOME-2A and GOME-2B data, which match each other well, but the features are also evident in the GOME-2C data despite the shorter period of coverage (not shown). The correlations between total H_2O data from the CAMS reanalysis and the NAO index agree very well with those from the GOME-2 satellite data. Good agreement also exists with the RD1SD model simulation results as shown in Figure 11d and in the supplement Figure S6 which shows the time series of NAO index and total H_2O anomalies from the RD1SD model simulation in winter for the long-term period 1979–2019. We note here

that the impact of NAO on total column water vapor has been assessed in previous studies, e.g., Fig. 12 of Trent et al. (2024), based on ERA-5 reanalysis data. The pattern of significant correlations we estimate between the NAO index and total H_2O column anomalies across the North Atlantic Ocean with GOME-2A, GOME-2B data, the CAMS reanalysis, and the EMAC RD1SD simulation closely resembles that presented by Trent et al. (2024).

The winter months of December, January, February, where the NAO is stronger, contribute significantly to the observed variability of the total H_2O column and largely shape the observed pattern of the estimated correlations shown in Figure 11. To investigate the changes of the total H_2O column associated with the NAO in winter, Figure 12 shows the time series of the H_2O anomalies along with the NAO index in winter, as December-January-February (DJF) mean, in two regions in the northern mid and high latitudes that show significant correlations: (a) Eastern Canada and the North Atlantic (50º–63º N, 40º–80º W), and (b) Northern Europe (50º–63º N, 10º W–30º E). Of particular interest is the strong negative phase of the NAO that occurred in the year 2010, which was one of the strongest in the past 40 years.

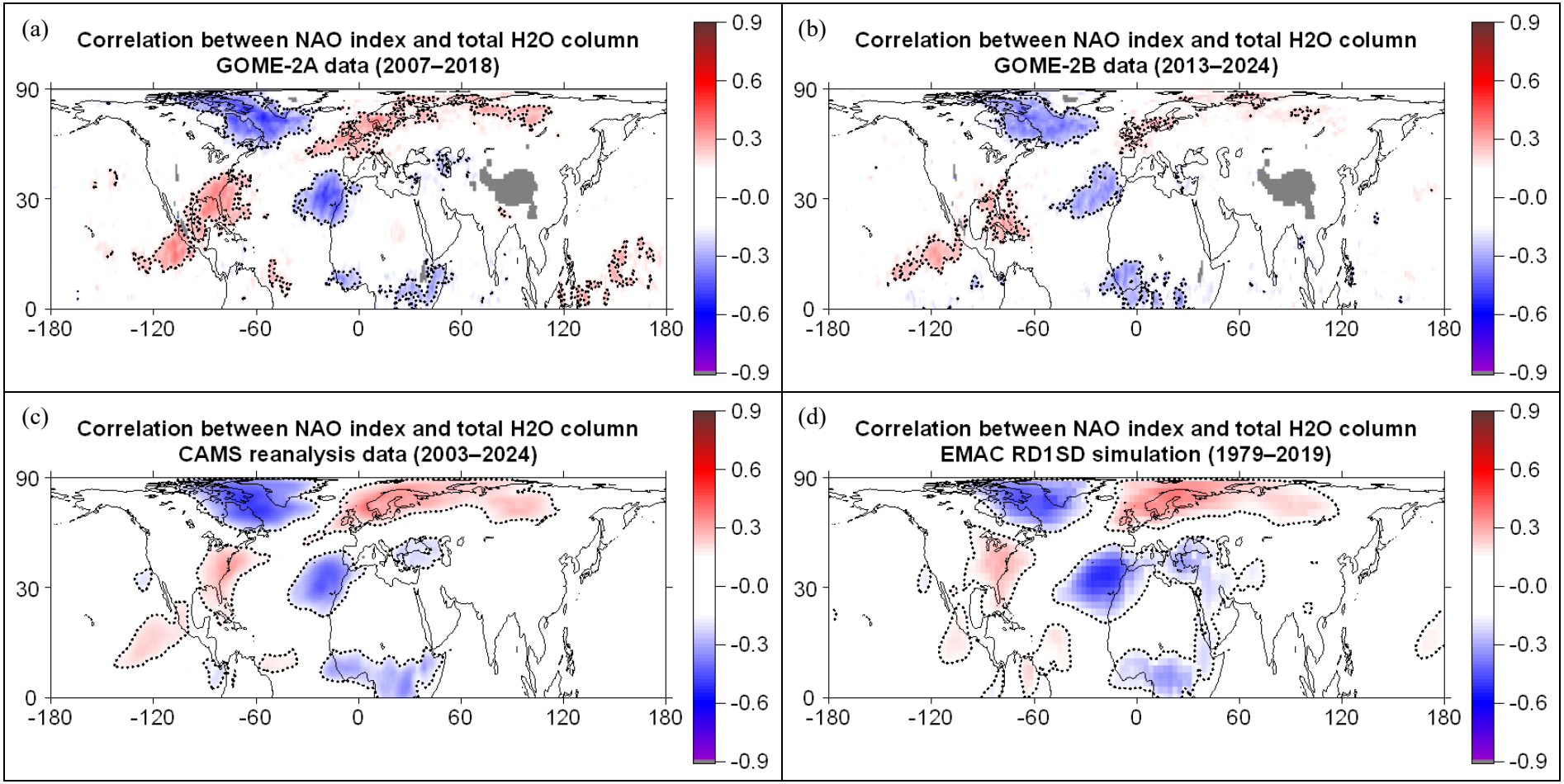

Fig. 11. Maps of correlation coefficients, *R*, between total H_2O column anomalies and the NAO index for (a) GOME-2A (2007-2018), (b) GOME-2B (2013-2023), (c) CAMS reanalysis (2003-2024) and (d) EMAC RD1SD simulation results (1979-2019). Only *R* above/below ±0.15 are shown. Dotted lines bound regions where *R* are statistically significant at C.L. 99%. Anomalies were calculated after removing the seasonal cycle and variability related to the QBO and ENSO.

The general picture in Northern Europe is that the variability of the H_2O column follows the NAO index, which suggests that positive H_2O anomalies (wetter conditions) are associated with a positive NAO index, while negative H_2O anomalies (drier conditions) are associated with a negative NAO index. Although this is not always the case, it is the case e.g. for winter 2010, where significant decreases of the H_2O column, i.e. very dry conditions, were observed in Northern Europe due to the strong negative NAO phase. Our results show that the strong negative phase of the NAO in the winter of 2010 had a strong impact on the H_2O column in the northern midlatitudes. According to Figure 12 we estimate that the total H_2O column increased significantly over Eastern Canada and the North Atlantic during the winter months of 2010 based on the GOME-2A data, by about 1.8 kg/m^2 or 45% of the mean, with the mean being about 4 kg/m^2. Over Northern Europe, on the other hand, H_2O decreased by about 0.8 kg/m^2 or 8% of the mean, with the mean being about 10 kg/m^2. This result, based on GOME-2A data, is smaller than that estimated from the CAMS data, which shows a decrease of about 1.8 kg/m^2 in 2010 and which appears to be consistent with the RD1SD model simulation results shown in Figure 12b. The correlation coefficient between CAMS and RD1SD total H_2O anomalies over Northern Europe is +0.97 (N=16, confidence level = 99.9%). Table 2 shows the correlation coefficients between GOME-2A, GOME-2B, CAMS and RD1SD total H_2O anomalies over Eastern Canada/North Atlantic and Northern Europe in winter (DJF mean).

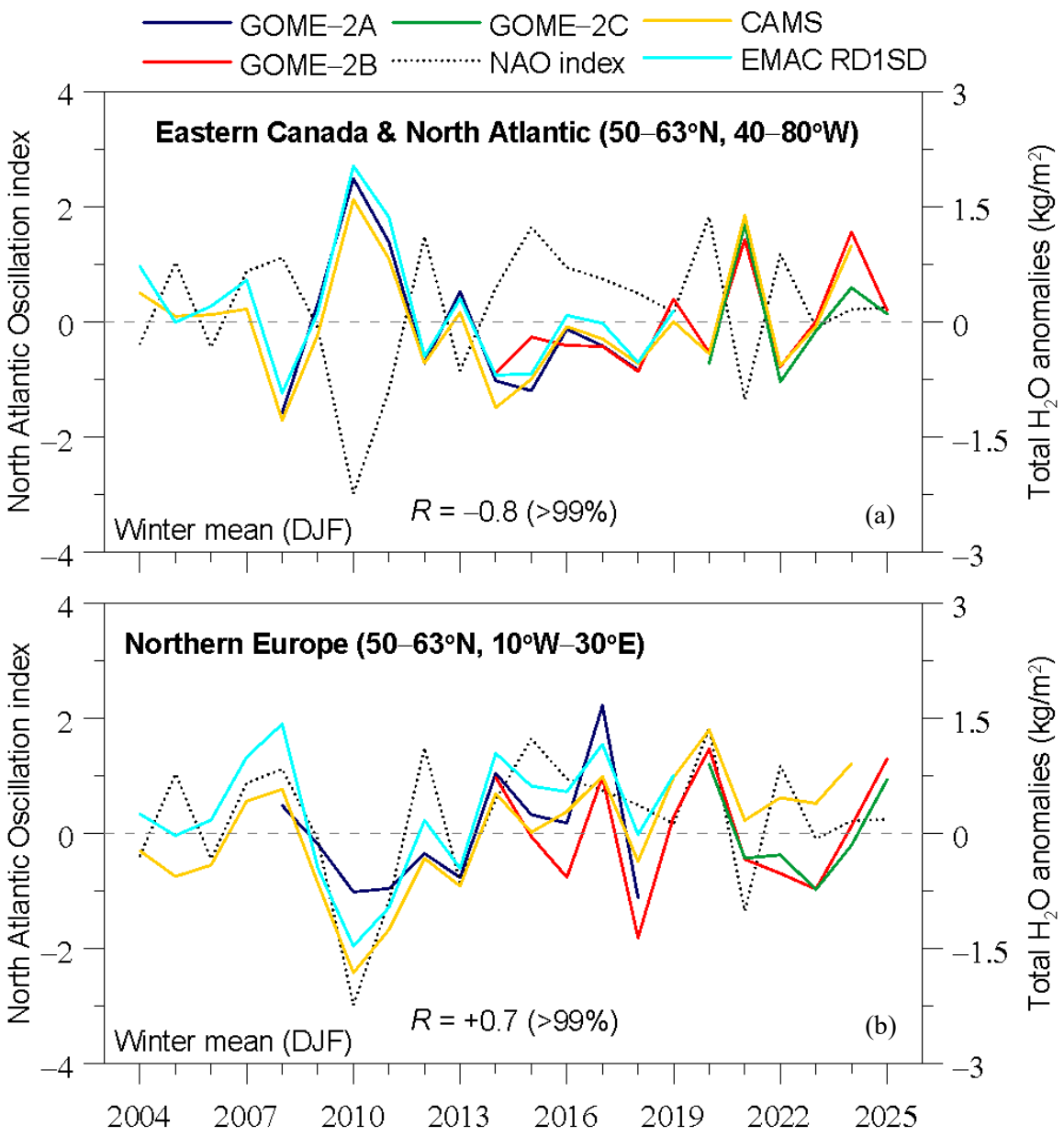

Fig. 12. Time series of total H_2O anomalies from GOME-2A, GOME-2B, GOME-2C data, CAMS reanalysis, and EMAC RD1SD simulation results along with the NAO index in DJF for: (a) Eastern Canada and the North Atlantic (50º–63º N, 40º–80º W), and (b) Northern Europe (50º–63º N, 10º W–30º E). *R* is the correlation coefficient between CAMS data and NAO index. Values in parentheses refer to statistical significance of *R*. Anomalies were calculated after removing the seasonal cycle and variability related to the QBO and ENSO.

(a) Eastern Canada and North Atlantic (50º–63º N, 40º–80º W)						
	Correlation	Slope*	Error	*t*-value	*p*-value	*N*
GOME-2A vs CAMS	0.978	1.070	0.080	14.162	<0.0001	11
GOME-2A vs RD1SD	0.986	0.899	0.051	17.678	<0.0001	11
GOME-2B vs CAMS	0.929	0.817	0.109	7.532	<0.0001	11
CAMS vs RD1SD	0.985	0.810	0.038	21.186	<0.0001	16
(b) Northern Europe (50º–63º N, 10º W–30º E)						
GOME-2A vs CAMS	0.822	0.781	0.180	4.335	0.00189	11
GOME-2A vs RD1SD	0.768	0.584	0.162	3.603	0.00572	11
GOME-2B vs CAMS	0.802	1.273	0.316	4.031	0.00297	11
CAMS vs RD1SD	0.974	0.794	0.049	16.086	<0.0001	16

Table 2. Statistics of correlations between total H_2O anomalies from GOME-2A, GOME-2B, CAMS reanalysis and EMAC RD1SD simulation for their common periods in winter (DJF mean), over (a) Eastern Canada and the North Atlantic (50º–63º N, 40º–80º W) and (b) Northern Europe (50º–63º N, 10º W–30º E). Anomalies were calculated after removing the seasonal cycle and variability related to the QBO and ENSO.

The case of winter 2010 (extreme negative NAO phase) has been investigated further. We have analyzed the spatial distribution of total H_2O anomalies over the North Atlantic and Europe during winter 2010 from CAMS reanalysis and the EMAC RD1SD simulation. The results are presented in Figure 13. Blue colors indicate increased dry conditions, and red colors indicate increased wet conditions due to the strong negative NAO phase. The agreement between CAMS data and RD1SD simulation results is quite high and the contrast between Northern and Southern Europe is quite clear. Northern Europe experienced drier winter conditions, while Southern Europe and the Mediterranean saw moister winter conditions. The highest positive H_2O anomalies were observed over western North Africa, the Canarian Islands, and the eastern parts of the North Atlantic. More specifically, in the region bounded by latitudes 25º – 35º N and longitudes 10º – 20º W, the mean anomalies exceeded 3 kg/m^2 or 19% of the long-term (2004–2024) mean, with the mean being about 16 kg/m^2. These estimates are based on CAMS reanalysis data. The respective numbers from the RD1SD simulation are 5 kg/m^2 or 28% of the long-term (1999–2019) mean, with the mean being about 18 kg/m^2. Large positive H_2O anomalies were also observed over the Eastern Canada and the northwestern parts of the North Atlantic Ocean. A similar analysis for an extreme positive NAO phase was not possible, as in the period under study there has been no extreme positive NAO phase event of comparable strength to the extreme negative NAO phase event of 2010.

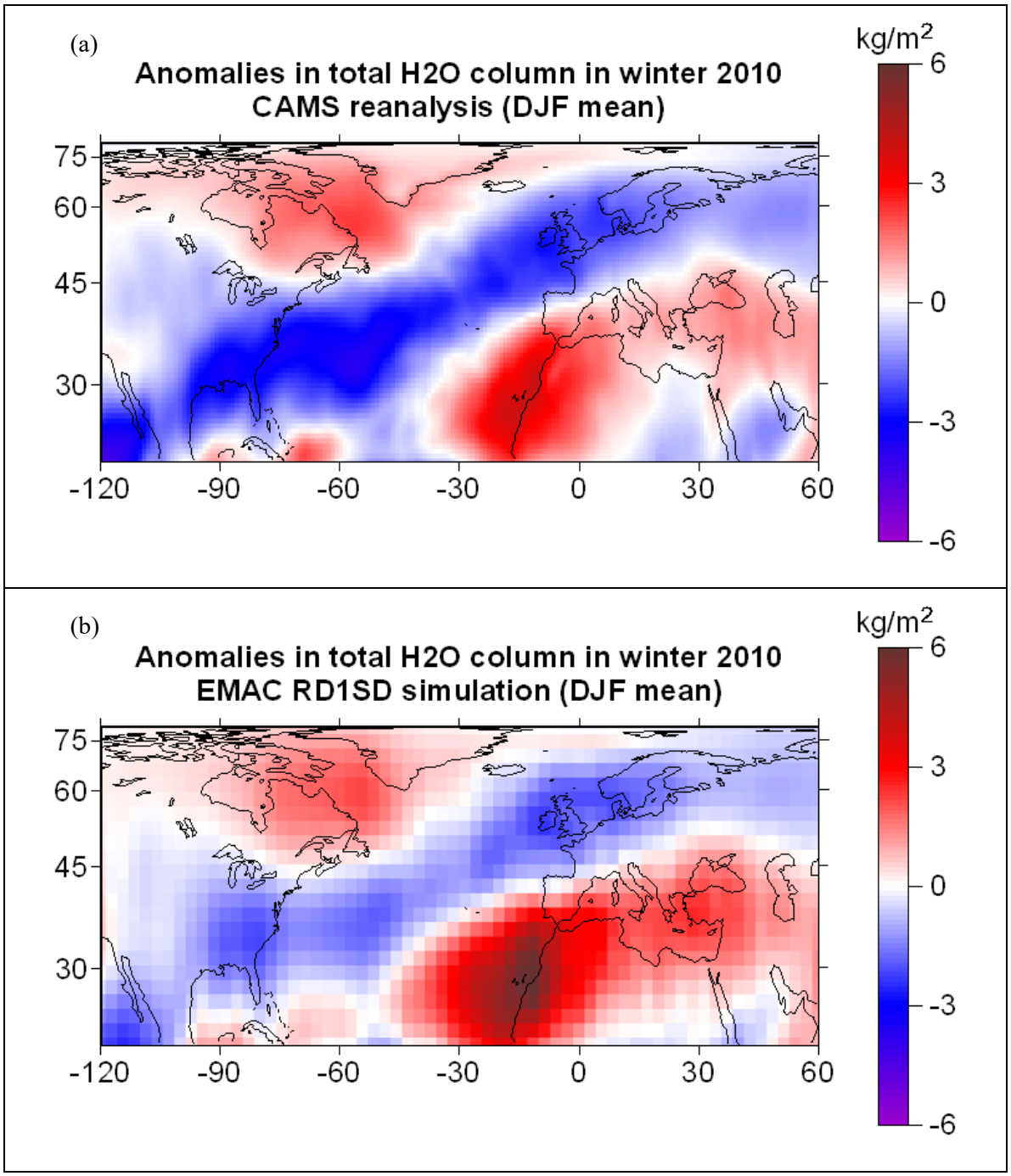

Fig. 13. Spatial distribution of total H_2O anomalies (kg/m^2) over the North Atlantic and Europe in winter 2010 (strong negative NAO phase) from (a) CAMS reanalysis and (b) EMAC RD1SD simulation. Anomalies were calculated after removing the seasonal cycle and variability related to the QBO and ENSO.

Going back to Figure 12 and the positive sign of correlation over Northern Europe, we note that the positive correlation between total H_2O and the NAO index is less pronounced in the GOME-2B data (period 2014–2025). Here, the correlation is estimated to be 0.25 and is statistically insignificant. The correlation between CAMS data and the NAO index also drops to 0.25 after 2014, which supports the GOME-2B results. It seems that after 2014 the relationship between NAO and total H_2O column weakens and that H_2O anomalies fluctuate more independently of the NAO, while before 2014 there was a clearer connection, i.e. H_2O anomalies were more tied to NAO behavior. There is little evidence in the literature on why the NAO appears with a less pronounced signal over Northern Europe after 2014. Recent studies estimate a weakening of the NAO variability in the future under high greenhouse gas emission scenario with implications on winter heavy precipitation events over Northern Europe (Fuentes-Franco et al., 2023). Mitevski et al. (2025) find a tendency towards more positive NAO values with increasing CO_2 concentrations, and also find a reduction in NAO variability, which leads to a smaller increase in the likelihood of extremely positive NAO events and a decrease in the frequency of extremely negative NAO events.

Reduction in NAO variability implies weaker NAO phases due to reduced pressure gradients between the Icelandic low-pressure and the Azores high-pressure systems, and might be the reason why we estimate a weaker correlation between total H_2O anomalies and the NAO index over Northern Europe in recent years, especially after 2014. We have calculated the correlation between the NAO index and total H_2O column anomalies before and after the year 2014 with the CAMS data. The results show that the correlation coefficient, R, for the period 2004–2013 is statistically significant at the 0.01 significance level (R = 0.82278, slope = 0.42893, error = 0.10476, t = 4.0945, p = 0.00346, N = 10), while the correlation coefficient for the period 2014–2024 is not statistically significant (R = 0.25099, slope = 0.13246, error = 0.17028, t = 0.77786, p = 0.4566, N = 11). We repeated the correlation analysis for the period 2004–2013 also without the year 2010, which could have affected our results due to the extremely strong negative NAO, and the results are still statistically significant (R = 0.66299, slope = 0.38537, error = 0.16947, t = 2.34312, p = 0.05161, N = 9). Moreover, application of a two-sample t-test for the difference between means in the CAMS data before and after 2014, shows that the

difference in mean H_2O column anomalies before and after 2014 over Northern Europe is statistically significant at the 0.05 significance level ($mean_{2004–2013} = –0.49107$, $mean_{2014–2024} = +0.47704$, $t = 3.75309$, $p = 0.00135$). Also, the variance of total H_2O column anomalies in the post-2014 period is smaller than in the pre-2014 period ($\sigma^2 = 0.21477$ in 2014–2024 and $\sigma^2 = 0.49717$ in 2004–2013). Their difference, however, based on the F-test for equality of variances, is not statistically significant at the 0.05 significance level but at the 0.15 significance level ($p = 0.1036$). The significantly lower H_2O before 2014 compared to after 2014 may have been affected by the exceptionally strong negative NAO in 2010, which was associated with much drier conditions. We repeated the statistical comparisons without the year 2010. The 2004–2013 average without 2010 is indeed smaller, but the difference between the two averages is still statistically significant. The results are as follows: ($mean_{2004–2013\ (no\ 2010)} = –0.34418$, $mean_{2014–2024} = +0.47704$, $t = 3.58316$, $p = 0.00213$). The variance for the period 2003–2014 excluding 2010 is now 0.31656, the variance for the period 2014–2024 is 0.21477 as before, and their difference is not statistically significant at the 0.05 significance level, as we also found when including the year 2010 in the analysis. Although the difference in the mean or variance in H_2O before and after 2014 is not directly related to the argument that the correlation between H_2O and NAO weakens after 2014, we keep in mind that a difference in basic statistical parameters of a variable, such as the mean or variance can provide possible indications that something may be changing in the variable. These statistical differences may reflect possible signs of observed reduced NAO variability, but since they are based on a small number of data in each sample, we cannot draw firm conclusions. We do not imply that the NAO will not continue to influence European climate, but our results may be an indication that seasonal weather anomalies in Northern Europe may be less related to the NAO and, as such, may be less well predicted by the NAO in the coming years.

Regarding the correlations between the NAO and total NO_2, there is also a good match between the GOME-2A and GOME-2B data in the northern extra tropics, with negative correlations across the North Atlantic Ocean towards Europe. The correlation maps between the NAO index and total NO_2 column anomalies from GOME-2A, 2B data are presented in Figures 14a and 14b, respectively. Figures 14c and 14d show the results

from the RD1SD model simulation for the periods 2007-2018 and 1979-2019, respectively, from which it appears that the model simulation agrees well with the GOME-2 data, with a path of negative correlations starting from the eastern US, crossing the North Atlantic on a northeasterly track reaching Europe.

We note here that although the correlations were performed with total column NO_2 data, they are most likely related to NAO effects on tropospheric column NO_2. It has been shown that NAO circulation patterns are an important governing factor for European wintertime composition and air pollution (Pope et al., 2018). Our results are in line with those findings. More specifically, in Figure S7 (supplement) we present the correlation between the NAO index and the total NO_2 and tropospheric NO_2 columns using all months in the correlation analysis and using the winter months of December, January and February. The results are based on the RD1SD model simulation for the long-term period 1979-2019. It appears that the pattern of correlation coefficients between the NAO index and total NO_2 column over North Atlantic and Europe using all months in the correlation analysis (panel a) is similar to that between NAO and the tropospheric NO_2 column (panel b), which points to tropospheric effects of NAO on the NO_2 column. Panels (c) and (d) show the respective correlations in winter (DJF mean), where it appears that the correlation coefficients in the North Atlantic and Europe are stronger in winter. These results support the results of Pope et al. (2018) on the influence of NAO on tropospheric composition over the North Atlantic and Europe and are consistent with their findings that NO_2 concentrations are reduced (enhanced) over Europe under the positive (negative) phase of NAO.

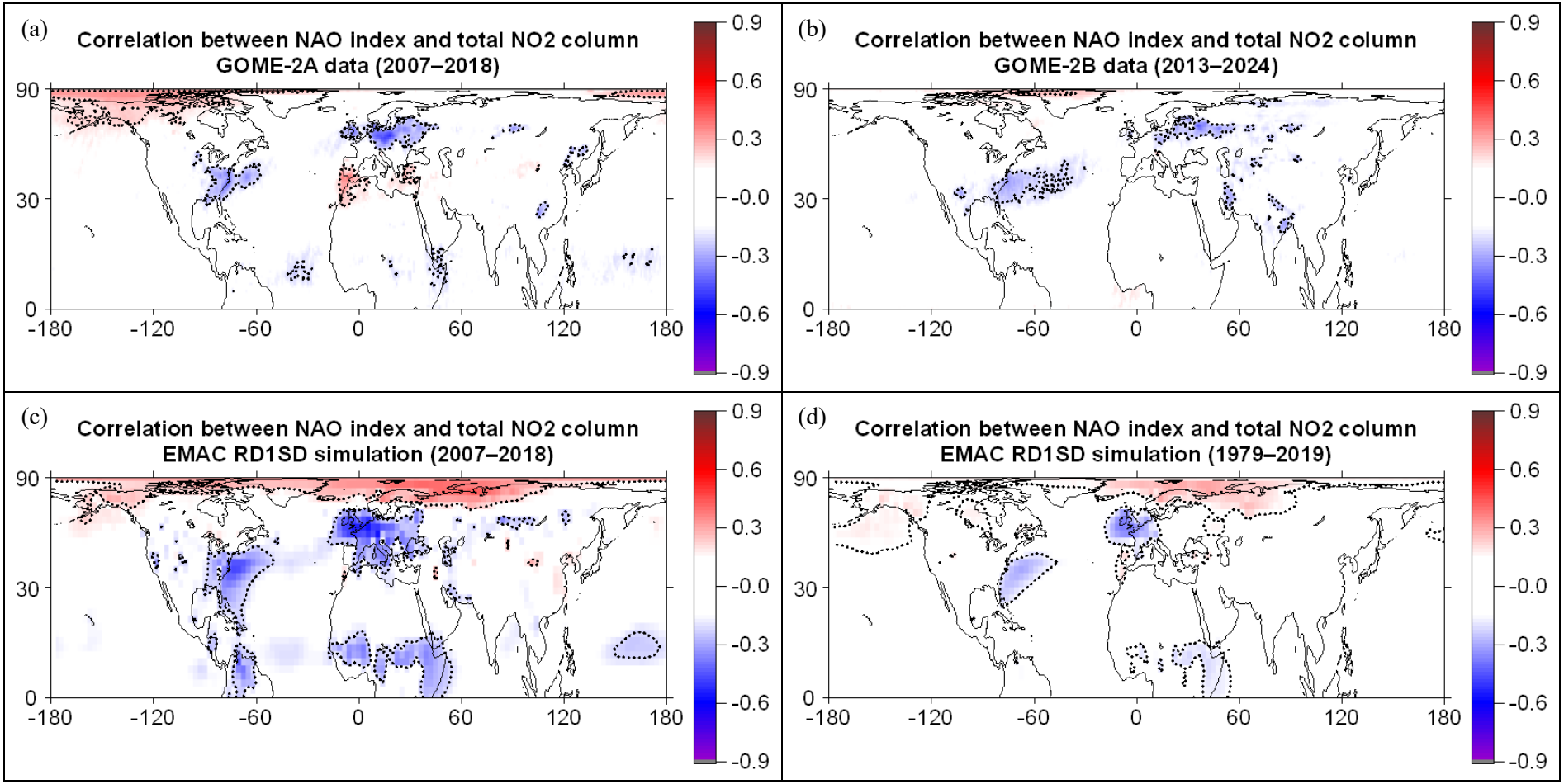

Fig. 14. Maps of correlation coefficients, R, between total NO_2 column anomalies and the NAO index for (a) GOME-2A (2007-2018), (b) GOME-2B (2013-2024), (c) EMAC RD1SD simulation (2007-2018) (common period with GOME-2A) and (d) EMAC RD1SD simulation results (1979-2019). Only *R* above/below ±0.15 are shown. Dotted lines bound regions where *R* are statistically significant at C.L. 99%. Anomalies were calculated after removing the seasonal cycle and variability related to the QBO and ENSO.

Christoudias et al. (2012) studied the emission and transport of tagged idealized tracers, with the characteristics of carbon monoxide (CO) and aerosols in the atmosphere, using the ECHAM5/MESSy1 Atmospheric Chemistry (EMAC) climate model. The authors showed that the phase of the NAO is significantly correlated with North American trace gases and aerosols over the northwestern Atlantic Ocean and across northern Europe, and with European trace gas and aerosol concentrations over Africa and north of the Arctic Circle. They also found that the NAO phase is strongly anti-correlated with European pollutant gas concentrations over western and central Europe. Our results for the tropospheric NO_2 column from the EMAC RD1SD simulation, shown in supplementary Figure S7d, show consistent patterns of correlations in winter (DJF) with those of Christoudias et al. (2012). More specifically, we find positive correlations between tropospheric NO_2 and the NAO index in northeastern Canada, northwest Atlantic, Iceland and northern Europe (Scandinavia), and north of the Arctic Circle, and positive correlations over North Africa although weaker ones. We also find significant negative correlations in central and Western Europe, and in the tropical Atlantic Ocean, which are in line with the results of Christoudias et al.

It should be noted however, that our results cannot be directly compared with those of Christoudias et al. This is because our results refer to the total NO_2 column, while in Christoudias et al. the correlations with the NAO were performed using CO as a trace gas. The correlation was presented for the model surface level and for the meridional vertical profile at 30°W. Also, the analysis of correlations was performed for tracer concentrations emitted separately from North America and separately from Europe (their Figures 7 and 8, respectively), which we do not do in the case of total NO_2. We note that we have chosen not to display correlation coefficients less than ±0.15 because they represent a small proportion of the variance explained by NAO (less than 2%). Nevertheless, despite these differences, the pattern of negative correlations observed in our maps, starting from the eastern US, crossing the North Atlantic towards Europe, is a consistent feature between our study and Christoudias et al. (2012).

Our analysis does not show different pattern of correlations between NAO and trace gas concentrations from that presented in previous studies. It does, however, analyze NO_2 column data from GOME-2 to see how the effect of NAO is captured in GOME-2A and

the newer versions, GOME-2B and GOME-2C, which were not done in previous studies. In view of recent studies showing that NAO will likely become more positive and less variable with increasing CO_2 concentrations, while extremely negative NAO events will decrease (Mitevski et al., 2025), it is expected that the upcoming changes to the NAO will have an impact on trace gas transport in the northern midlatitudes, influencing transboundary pollution between North America and Europe. Climate model simulations of the NAO signal and trends in the future and its influence on air pollution transport over the North Atlantic sector by Bacer et al. (2016) suggest that at the end of the century, the southwestern Mediterranean and northern Africa will have enhanced pollutant concentrations during positive NAO phases, while northern Europe will have reduced pollutant concentrations. Although we do assess the evolution of the total NO_2 column into the future, we believe that the consistency between the GOME-2B and GOME-2C total NO_2 columns in terms of NAO-related variability will be useful in studies quantifying changes in trace gas columns in the North Atlantic in the coming years and in verifying atmospheric model simulations with GOME-2 data.

4. Summary and Conclusions

We have studied correlations between major low-frequency oscillations in the Earth's atmosphere, Quasi-Biennial Oscillation (QBO), El Niño Southern Oscillation (ENSO), and North Atlantic Oscillation (NAO), and total columns of NO_2 and H_2O retrieved from measurements taken by three GOME-2 sensors (GOME-2A, GOME-2B, and GOME-2C). The results were compared to CAMS reanalysis (H_2O only) and the RD1SD simulation from the EMAC chemistry-climate model. We find distinct spatial patterns of significant correlations between the three indices and the trace gases (except between the QBO and H_2O), which are consistent among these datasets. We generally conclude that GOME-2 data, CAMS and the EMAC model are useful for studies related to trace gases. Our findings can be summarized as follows.

The results show that the stratospheric QBO is well depicted in the GOME-2A/B/C L3 total NO_2 column retrievals. The correlation coefficients between QBO and total NO_2 are larger in the tropics (10°W–10°E) and smaller in the extra tropics in agreement with previous studies. We investigated the impact of QBO disruptions in 2015-16 and 2019-20 on the variability of total NO_2 from GOME-2 and found reductions in the total column NO_2 during periods with QBO disruption compared to periods without QBO disruption. This result was corroborated by additional analysis of OMI satellite data. On the other hand, correlations between total H_2O and the QBO were small and statistically insignificant. Analysis of total H_2O data from the independently produced CAMS reanalysis confirmed this result.

The effects of ENSO on total H_2O column from GOME-2 are evident in the tropical Pacific Ocean, while the effect of NAO is evident in the northern midlatitudes. The variability of total H_2O from GOME-2 has been compared with that from CAMS and good agreement is found between these datasets. In the eastern Tropical Pacific Ocean, total H_2O column increases during El Niño events and decreases during La Niña events while the opposite is observed in the western part of the Tropical Pacific Ocean. During the strong El Niño event of 2015-16, total H_2O increased up to about 10 kg/m^2 in the eastern tropical Pacific corresponding to about 25% of the mean, with the mean being about 40 kg/m^2. In its western part, the H_2O column decreased by a comparable amount

(about 14% of the mean). Such studies help us to understand the magnitude of changes of the total H_2O column during recent ENSO events. The agreement we find between GOME-2A and GOME-2B H_2O anomalies during the major El Niño event of 2015-16 and between GOME-2B and GOME-2C H_2O anomalies during the recent major El Niño event of 2023-24 and the prolonged La Niña event of 2020-23 indicates that data from the newer GOME-2 instruments can be quite reliable for quantifying changes in water vapor during upcoming El Niño and La Niña events, the frequency and duration of which have shown increasing trends in the last years. The respective correlation analysis between ENSO and total NO_2 showed statistically significant correlation coefficients over the Indonesian area and the central and eastern Tropical Pacific Ocean, the majority of which was within ±0.4. During strong El Niño events, total column NO_2 from GOME-2 increases over Indonesia and decreases in central/eastern Tropical Pacific Ocean in agreement with previous studies.

The NAO is negatively correlated with the variability of the total H_2O column over eastern Canada and the North Atlantic (R= –0.8), and positively correlated over northern Europe (R= +0.7). These estimates are based on CAMS reanalysis data for the period 2003-2024 in winter and are consistent with GOME-2A results. During the strong negative phase of the NAO in the winter of 2010, the total H_2O column increased significantly during the winter months of 2010 based on GOME-2A, by about 1.8 kg/m^2 or 45% of the mean, with the mean being about 4 kg/m^2. Over Northern Europe, on the other hand, H_2O decreased by about 0.8 kg/m^2 or 8% of the mean, with the mean being about 10 kg/m^2. A notable finding from our analysis is that the positive correlation between total H_2O and the NAO index over northern Europe in winter decreases after 2014 and is statistically insignificant (R= +0.25). This is evident from GOME-2B and CAMS data and may be related to recent findings suggesting a weakening of NAO variability with increasing CO_2 concentrations.

The variability of total H_2O from GOME-2 in regions affected by ENSO and NAO was also compared with the RD1SD simulation results from the ECHAM/MESSy Atmospheric Chemistry (EMAC) model. It was found that the magnitude of total H_2O changes during warm (El Niño) and cold (La Niña) ENSO events from the model simulation, as well as changes of total H_2O related to the NAO, agree well with the

satellite measurements. With regard to the correlations between total NO_2 from GOME-2 and the NAO, the results showed negative correlations with the NAO, along a path starting from the eastern US, crossing the North Atlantic on a northeasterly track reaching Europe. A similar pattern of correlations was also found with the RD1SD model simulation results. Our findings are consistent with those of previous studies.

In conclusion, we find that quasi-cyclical fluctuations, QBO, ENSO, and NAO, are well reflected in the variability of total NO_2 and H_2O columns from GOME-2 (except QBO in H_2O). Analysis of the CAMS reanalysis and EMAC RD1SD model simulation results show that the model data are in qualitative and quantitative agreement with the GOME-2 satellite data, verifying the good quality of the reanalysis data and model simulation results to be used in atmospheric research and climate studies related to total NO_2 and total H_2O column changes. In view of recent studies demonstrating anomalies or changes in the regular cycle of QBO, ENSO, NAO (e.g., Anstey et al., 2021; Lu et al. 2025; Mitevski et al., 2025) our main message is that data from the newer versions of the GOME-2 instrument, GOME-2B and GOME-2C, can be quite useful for examining the response of NO_2 and H_2O to potential anomalies or changes in the QBO/ENSO/NAO signals in the near future and can advance our knowledge in the representation of these natural cycles in climate model simulations of trace gases in the coming years.

Acknowledgements

The study has been funded by the European Organization for the Exploitation of Meteorological Satellites (EUMETSAT) in the framework of the Satellite Application Facility on Atmospheric Composition Monitoring (AC SAF) Continuous Development and Operations Phase 4 (CDOP4) and national contributions. We acknowledge support of this work by the Mariolopoulos-Kanaginis Foundation for the Environmental Sciences. We acknowledge DLR-IMF for providing the monthly GOME-2 L3 trace gas column data and for their support.

The EMAC model simulations have been performed at the German Climate Computing Centre (DKRZ) through support from the Bundesministerium für Bildung und Forschung (BMBF). DKRZ and its scientific steering committee are gratefully

acknowledged for providing the HPC and data archiving resources for this consortial project ESCiMo (Earth System Chemistry integrated Modelling).

Data Availability Statement.

GOME-2 Level 3 (L3) trace gas column data from the ACSAF project are available at https://acsaf.org/. Total H_2O column data from CAMS global reanalysis (EAC4) are available at https://ads.atmosphere.copernicus.eu/datasets/cams-global-reanalysis-eac4?tab=overview. EMAC RD1SD data are available at https://doi.org/10.26050/WDCC/ESCiMo2_RD1SD (Jöckel et al., 2024a) and https://www.wdc-climate.de/ui/entry?acronym=DKRZ_LTA_853_dsg0002 (Jöckel et al., 2024b). Zonal winds in Singapore at 10 and 30 hPa (QBO10 and QBO30) by NASA/GSFC Atmospheric Chemistry and Dynamics Laboratory are available at https://acd-ext.gsfc.nasa.gov/Data_services/met/qbo/qbo.html#links. The Niño anomaly 3.4 index (Niño3.4) by the NOAA Physics Sciences Laboratory is available at https://psl.noaa.gov/data/climateindices/list/. North Atlantic Oscillation (NAO) Index (PC-based) by Jim Hurrell at NCAR is available at https://climatedataguide.ucar.edu/climate-data/hurrell-north-atlantic-oscillation-nao-index-pc-based.

REFERENCES

Anglou, I., Glissenaar, I. A., Boersma, K. F., and Eskes, H., 2024: ESA CCI+ OMI L3 monthly mean NO2 columns [Data set], Royal Netherlands Meteorological Institute (KNMI), doi:10.21944/cci-no2-omi-l3.

Anstey, J. A., Banyard, T. P., Butchart, N., Coy, L., Newman, P. A., Osprey, S., and Wright, C. J., 2021: Prospect of increased disruption to the QBO in a changing climate, *Geophysical Research Letters*, **48**, e2021GL093058, https://doi.org/10.1029/2021GL093058.

Bai, X., Wang, Y., Gui, L., Tao, M., and Zeng, M., 2025: Comparing the Influences on NO_2 Changes in Terms of Inter-Annual and Seasonal Variations in Different Regions of

China: Meteorological and Anthropogenic Contributions, *Remote Sensing*, **17**(1), 121, https://doi.org/10.3390/rs17010121.

Baldwin, M. P., Gray, L. J., Dunkerton, T. J., Hamilton, K., Haynes, P. H., Randel, W. J., Holton, J. R., Alexander, M. J., Hirota, I., Horinouchi, T., Jones, D. B. A., Kinnersley, J. S., Marquardt, C., Sato, K., and Takahashi, M., 2001: The quasi-biennial oscillation. *Rev. Geophys.*, **39**, 179–229, https://doi.org/10.1029/1999RG000073.

Banyard, T. P., Wright, C. J., Osprey, S. M., Hindley, N. P., Halloran, G., Coy, L., Newman, P. A., Butchart, N., Bramberger, M., and Alexander, M. J., 2024: Aeolus wind lidar observations of the 2019/2020 quasi-biennial oscillation disruption with comparison to radiosondes and reanalysis, *Atmos. Chem. Phys.*, **24**, 2465–2490, https://doi.org/10.5194/acp-24-2465-2024.

Beirle, S., Lampel, J., Wang, Y., Wagner, T., Grossi, M., and Loyola, D., 2018: The GOME-Evolution total column water vapor "climate" product (Version 2.2). World Data Center for Climate (WDCC) at DKRZ. https://doi.org/10.1594/WDCC/GOME-EVL_water_vapor_clim_v2.2.

Boynard, A., Hurtmans, D., Garane, K., Goutail, F., Hadji-Lazaro, J., Koukouli, M. E., Wespes, C., Vigouroux, C., Keppens, A., Pommereau, J.-P., Pazmino, A., Balis, D., Loyola, D., Valks, P., Sussmann, R., Smale, D., Coheur, P.-F., and Clerbaux, C., 2018: Validation of the IASI FORLI/EUMETSAT ozone products using satellite (GOME-2), ground-based (Brewer–Dobson, SAOZ, FTIR) and ozonesonde measurements. *Atmos. Meas. Tech.*, **11**, 5125–5152, https://doi.org/10.5194/amt-11-5125-2018.

Brenot, H., Theys, N., Clarisse, L., van Geffen, J., van Gent, J., Van Roozendael, M., van der A, R., Hurtmans, D., Coheur, P.-F., Clerbaux, C., Valks, P., Hedelt, P., Prata, F., Rasson, O., Sievers, K., and Zehner, C., 2014: Support to Aviation Control Service (SACS): an online service for near-real-time satellite monitoring of volcanic plumes. *Nat. Hazards Earth Syst. Sci.*, **14**, 1099–1123, https://doi.org/10.5194/nhess-14-1099-2014.

Brohede, S., McLinden, C. A., Urban, J., Haley, C. S., Jonsson, A. I., and Murtagh, D., 2008: Odin stratospheric proxy NOy measurements and climatology, *Atmos. Chem. Phys.*, **8**, 5731–5754, https://doi.org/10.5194/acp-8-5731-2008.

Cai, W., Borlace, S., Lengaigne, M., van Rensch, P., Collins, M., Vecchi, G., Timmermann, A., Santoso, A., McPhaden, M. J., Wu. L., England, M. H., Wang, G., Guilyardi, E., and Jin, F.-F., 2014: Increasing frequency of extreme El Niño events due to greenhouse warming, *Nature Climate Change*, **4**, 111–116, https://doi.org/10.1038/nclimate2100.

Cai, W., Ng, B., Geng, T., Jia, F., Wu, L., Wang, G., Liu, Y., Gan, B., Yang, K., Santoso, A., Lin, X., Li, Z., Liu, Y., Yang, Y., Jin, F.-F., Collins, M., and McPhaden M. J., 2023: Anthropogenic impacts on twentieth-century ENSO variability changes, *Nature Reviews Earth & Environment*, **4**, 407–418, https://doi.org/10.1038/s43017-023-00427-8.

Ceppi, P., and Fueglistaler, S., 2021: The El Niño–Southern Oscillation pattern effect. *Geophys. Res. Lett.*, **48**, e2021GL095261, https://doi.org/10.1029/2021GL095261.

Chabrillat, S., Rémy, S., Errera, Q., Huijnen, V., Bingen, C., Debosscher, J., Hendrick, F., Metzger, S., Mora, A., Minganti, D., Op de beek, M., Reisenfeld, L., Williams, J. E., Eskes, H., and Flemming, J., 2025: Modelling stratospheric composition for the Copernicus Atmosphere Monitoring Service: multi-species evaluation of IFS-COMPO Cy49R1, EGUsphere [preprint], https://doi.org/10.5194/egusphere-2025-1327.

Chan, K. L., Valks, P., Slijkhuis, S., Köhler, C., and Loyola, D., 2020: Total column water vapor retrieval for Global Ozone Monitoring Experience-2 (GOME-2) visible blue observations. *Atmos. Meas. Tech.*, **13**, 4169–4193, https://doi.org/10.5194/amt-13-4169-2020.

Chan, K. L., Valks, P., Heue, K.-P., Lutz, R., Hedelt, P., Loyola, D., Pinardi, G., Van Roozendael, M., Hendrick, F., Wagner, T., Kumar, V., Bais, A., Piters, A., Irie, H., Takashima, H., Kanaya, Y., Choi, Y., Park, K., Chong, J., Cede, A., Frieß, U., Richter, A., Ma, J., Benavent, N., Holla, R., Postylyakov, O., Rivera Cárdenas, C., and Wenig, M., 2023: Global Ozone Monitoring Experiment-2 (GOME-2) daily and monthly level-3 products of atmospheric trace gas columns. *Earth Syst. Sci. Data*, **15**, 1831–1870, https://doi.org/10.5194/essd-15-1831-2023.

Chang, L.-S., Kim, D., Hong, H., Kim, D.-R., Yu, J.-A., Lee, K., Lee, H., Kim, D., Hong, J., Jo, H.-Y., and Kim, C.-H., 2022: Evaluation of correlated Pandora column NO_2 and in situ surface NO_2 measurements during GMAP campaign, *Atmos. Chem. Phys.*, **22**, 10703–10720, https://doi.org/10.5194/acp-22-10703-2022.

Chipperfield, M. P., Gray, L. J., Kinnersley, J. S., and Zawodny, J., 1994: A two-dimensional model study of the QBO signal in SAGE II NO2 and O3, *Geophys. Res. Lett.*, **21**, 589–592.

Chiou, E. W., Bhartia, P. K., McPeters, R. D., Loyola, D. G., Coldewey-Egbers, M., Fioletov, V. E., Van Roozendael, M., Spurr, R., Lerot, C., and Frith, S. M., 2014: Comparison of profile total ozone from SBUV (v8.6) with GOME-type and ground-based total ozone for a 16-year period (1996 to 2011). *Atmos. Meas. Tech.*, **7**, 1681–1692, https://doi.org/10.5194/amt-7-1681-2014.

Choi, W., Lee, H., Grant, W. B., Park, J. H., Holton, J. R., Lee, K. M., and Naujokat, B., 2002: On the secondary meridional circulation associated with the quasi-biennial oscillation, *Tellus B.*, **54**, 395-406, https://doi.org/10.1034/j.1600-0889.2002.201286.x.

Christoudias, T., Pozzer, A., and Lelieveld, J., 2012: Influence of the North Atlantic Oscillation on air pollution transport, *Atmos. Chem. Phys.*, **12**, 869-877, https://doi.org/10.5194/acp-12-869-2012.

Chtirkova, B., Folini, D., Correa, L. F., and Wild, M., 2023: Internal variability of the climate system mirrored in decadal-scale trends of surface solar radiation. *Journal of Geophysical Research: Atmospheres*, **128**, e2023JD038573. https://doi.org/10.1029/2023JD038573.

Coldewey-Egbers, M., Loyola R., D. G., Braesicke, P., Dameris, M., van Roozendael, M., Lerot, C., and Zimmer, W., 2014: A new health check of the ozone layer at global and regional scales. *Geophys. Res. Lett.*, **41**, 4363–4372, doi:10.1002/2014GL060212.

Coy, L., Newman, P. A., Pawson, S., and Lait, L. R., 2017: Dynamics of the Disrupted 2015/16 Quasi-Biennial Oscillation. *J. Climate*, **30**, 5661–5674, https://doi.org/10.1175/JCLI-D-16-0663.1.

Crutzen, P. J., 1979: The role of NO and NO2 in the chemistry of the troposphere and stratosphere, *Ann. Rev. Earth Planet Sci.*, **7**, 443-472.

De Smedt, I., Stavrakou, T., Hendrick, F., Danckaert, T., Vlemmix, T., Pinardi, G., Theys, N., Lerot, C., Gielen, C., Vigouroux, C., Hermans, C., Fayt, C., Veefkind, P., Müller, J.-F., and Van Roozendael, M., 2015: Diurnal, seasonal and long-term variations of global formaldehyde columns inferred from combined OMI and GOME-2 observations. *Atmos. Chem. Phys.*, **15**, 12519–12545, https://doi.org/10.5194/acp-15-12519-2015.

Dirksen, R. J., Boersma, K. F., Eskes, H. J., Ionov, D. V., Bucsela, E. J., Levelt, P. F., and Kelder, H. M., 2011: Evaluation of stratospheric NO2 retrieved from the Ozone Monitoring Instrument: Intercomparison, diurnal cycle, and trending. *Journal of Geophysical Research: Atmospheres*, **116**, D08305, doi:10.1029/2010JD014943.

Dubé, K., Randel, W., Bourassa, A., Zawada, D., McLinden, C., and Degenstein, D., 2020: Trends and variability in stratospheric NOx derived from merged SAGE II and OSIRIS satellite observations. *Journal Geophysical Research: Atmospheres*, **125**, e2019JD031798. https://doi.org/10.1029/2019JD031798.

Eleftheratos, K., Zerefos, C. S., Zanis, P., Balis, D. S., Tselioudis, G., Gierens, K., and Sausen, R., 2007: A study on natural and manmade global interannual fluctuations of cirrus cloud cover for the period 1984–2004. *Atmos. Chem. Phys.*, **7**, 2631–2642, https://doi.org/10.5194/acp-7-2631-2007.

Eleftheratos, K., Zerefos, C. S., Balis, D. S., Koukouli, M.-E., Kapsomenakis, J., Loyola, D. G., Valks, P., Coldewey-Egbers, M., Lerot, C., Frith, S. M., Haslerud, A. S., Isaksen, I. S. A., and Hassinen, S., 2019: The use of QBO, ENSO, and NAO perturbations in the evaluation of GOME-2 MetOp A total ozone measurements. *Atmos. Meas. Tech.*, **12**, 987–1011, https://doi.org/10.5194/amt-12-987-2019.

Field, R. D., van der Werf, G. R., Fanin, T., Fetzer, E. J., Fuller, R., Jethva, H., Levy, R., Livesey, N. J., Luo, M., Torres, O., and Worden, H. M., 2016: Indonesian fire activity and smoke pollution in 2015 show persistent nonlinear sensitivity to El Niño-induced drought, *PNAS*, vol. **113**, no. 33, 9204-9209.

Garane, K., Koukouli, M.-E., Verhoelst, T., Lerot, C., Heue, K.-P., Fioletov, V., Balis, D., Bais, A., Bazureau, A., Dehn, A., Goutail, F., Granville, J., Griffin, D., Hubert, D., Keppens, A., Lambert, J.-C., Loyola, D., McLinden, C., Pazmino, A., Pommereau, J.-P., Redondas, A., Romahn, F., Valks, P., Van Roozendael, M., Xu, J., Zehner, C., Zerefos, C., and Zimmer, W., 2019: TROPOMI/S5P total ozone column data: global ground-based validation and consistency with other satellite missions. *Atmos. Meas. Tech.*, **12**, 5263–5287, https://doi.org/10.5194/amt-12-5263-2019.

Gaudel, A., Cooper, O. R., Ancellet, G., Barret, B., Boynard, A., Burrows, J. P., Clerbaux, C., Coheur, P.-F., Cuesta, J., Cuevas, E., Doniki, S., Dufour, G., Ebojie, F., Foret, G., Garcia, O., Granados-Muñoz, M. J., Hannigan, J. W., Hase, F., Hassler, B., Huang, G.,

Hurtmans, D., Jaffe, D., Jones, N., Kalabokas, P., Kerridge, B., Kulawik, S., Latter, B., Leblanc, T., Le Flochmoën, E., Lin, W., Liu, J., Liu, X., Mahieu, E., McClure-Begley, A., Neu, J. L., Osman, M., Palm, M., Petetin, H., Petropavlovskikh, I., Querel, R., Rahpoe, N., Rozanov, A., Schultz, M. G., Schwab, J., Siddans, R., Smale, D., Steinbacher, M., Tanimoto, H., Tarasick, D. W., Thouret, V., Thompson, A. M., Trickl, T., Weatherhead, E., Wespes, C., Worden, H. M., Vigouroux, C., Xu, X., Zeng, G., and Ziemke, J., 2018: Tropospheric Ozone Assessment Report: Present-day distribution and trends of tropospheric ozone relevant to climate and global atmospheric chemistry model evaluation. *Elementa: Science of the Anthropocene*, **6**: 39, doi: https://doi.org/10.1525/elementa.291.

Grossi, M., Valks, P., Loyola, D., Aberle, B., Slijkhuis, S., Wagner, T., Beirle, S., and Lang, R., 2015: Total column water vapour measurements from GOME-2 MetOp-A and MetOp-B. *Atmos. Meas. Tech.*, **8**, 1111–1133, https://doi.org/10.5194/amt-8-1111-2015.

Hao, N., Koukouli, M. E., Inness, A., Valks, P., Loyola, D. G., Zimmer, W., Balis, D. S., Zyrichidou, I., Van Roozendael, M., Lerot, C., and Spurr, R. J. D., 2014: GOME-2 total ozone columns from MetOp-A/MetOp-B and assimilation in the MACC system. *Atmos. Meas. Tech.*, **7**, 2937–2951, https://doi.org/10.5194/amt-7-2937-2014.

Hassinen, S., Balis, D., Bauer, H., Begoin, M., Delcloo, A., Eleftheratos, K., Gimeno Garcia, S., Granville, J., Grossi, M., Hao, N., Hedelt, P., Hendrick, F., Hess, M., Heue, K.-P., Hovila, J., Jønch-Sørensen, H., Kalakoski, N., Kauppi, A., Kiemle, S., Kins, L., Koukouli, M. E., Kujanpää, J., Lambert, J.-C., Lang, R., Lerot, C., Loyola, D., Pedergnana, M., Pinardi, G., Romahn, F., van Roozendael, M., Lutz, R., De Smedt, I., Stammes, P., Steinbrecht, W., Tamminen, J., Theys, N., Tilstra, L. G., Tuinder, O. N. E., Valks, P., Zerefos, C., Zimmer, W., and Zyrichidou, I., 2016: Overview of the O3M SAF GOME-2 operational atmospheric composition and UV radiation data products and data availability. *Atmos. Meas. Tech.*, **9**, 383–407, https://doi.org/10.5194/amt-9-383-2016.

Hersbach, H., Bell, B., Berrisford, P., Hirahara, S., Horányi, A., Muñoz-Sabater, J., Nicolas, J., Peubey, C., Radu, R., Schepers, D., Simmons, A., Soci, C., Abdalla, S., Abellan, X., Balsamo, G., Bechtold, P., Biavati, G., Bidlot, J., Bonavita, M., De Chiara, G., Dahlgren, P., Dee, D., Diamantakis, M., Dragani, R., Flemming, J., Forbes, R., Fuentes, M., Geer, A., Haimberger, L., Healy, S., Hogan, R. J., Hólm, E., Janisková, M., Keeley,

S., Laloyaux, P., Lopez, P., Lupu, C., Radnoti, G., de Rosnay, P., Rozum, I., Vamborg, F., Villaume, S., and Thépaut, J.-N., 2020: The ERA5 global reanalysis. *Q J R Meteorol Soc.*, **146**, 1999–2049, https://doi.org/10.1002/qj.3803.

Hogikyan, A., Resplandy, L., and Fueglistaler, S., 2022: Cause of the intense tropics-wide tropospheric warming in response to El Niño. *Journal of Climate*, **35**(10), 2933–2944, https://doi.org/10.1175/JCLI-D-21-0728.1.

Huijnen, V., Wooster, M. J., Kaiser, J. W., Gaveau, D. L. A., Flemming, J., Parrington, M., Inness, A., Murdiyarso, D., Main, B., and van Weele, M., 2016: Fire carbon emissions over maritime southeast Asia in 2015 largest since 1997, *Scientific Reports*, **6**, 26886, https://doi.org/10.1038/srep26886.

Hurrell, J. W., Kushnir, Y., Ottersen, G. and Visbeck, M., 2003: An Overview of the North Atlantic Oscillation. *In The North Atlantic Oscillation: Climatic Significance and Environmental Impact* (eds J.W. Hurrell, Y. Kushnir, G. Ottersen and M. Visbeck). https://doi.org/10.1029/134GM01.

Hurrell, James &, Phillips, Adam & National Center for Atmospheric Research Staff (Eds). Last modified 2025-08-25 "The Climate Data Guide: Hurrell North Atlantic Oscillation (NAO) Index (PC-based)." Retrieved from https://climatedataguide.ucar.edu/climate-data/hurrell-north-atlantic-oscillation-nao-index-pc-based on 2025-10-13.

Inness, A., Benedetti, A., Flemming, J., Huijnen, V., Kaiser, J. W., Parrington, M., and Remy, S., 2015: The ENSO signal in atmospheric composition fields: emission-driven versus dynamically induced changes. *Atmos. Chem. Phys.*, **15**, 9083–9097, https://doi.org/10.5194/acp-15-9083-2015.

Inness, A., Ades, M., Agustí-Panareda, A., Barré, J., Benedictow, A., Blechschmidt, A.-M., Dominguez, J. J., Engelen, R., Eskes, H., Flemming, J., Huijnen, V., Jones, L., Kipling, Z., Massart, S., Parrington, M., Peuch, V.-H., Razinger, M., Remy, S., Schulz, M., and Suttie, M., 2019: The CAMS reanalysis of atmospheric composition. *Atmos. Chem. Phys.*, **19**, 3515–3556, https://doi.org/10.5194/acp-19-3515-2019.

Jöckel, P., Tost, H., Pozzer, A., Kunze, M., Kirner, O., Brenninkmeijer, C. A. M., Brinkop, S., Cai, D. S., Dyroff, C., Eckstein, J., Frank, F., Garny, H., Gottschaldt, K.-D., Graf, P., Grewe, V., Kerkweg, A., Kern, B., Matthes, S., Mertens, M., Meul, S., Neumaier, M., Nützel, M., Oberländer-Hayn, S., Ruhnke, R., Runde, T., Sander, R., Scharffe, D., and

Zahn, A., 2016: Earth System Chemistry integrated Modelling (ESCiMo) with the Modular Earth Submodel System (MESSy) version 2.51. *Geosci. Model Dev.*, **9**, 1153–1200, https://doi.org/10.5194/gmd-9-1153-2016.

Jöckel, P., Brinkop, S., Graf, P., Eichinger, R., Garny, H., Mertens, M., Nützel, M., Pozzer, A., Tost, H., and the MESSy Consortium, 2024a: RD1SD: EMAC CCMI-2022 hindcast simulations with specified dynamics, ERA-5, 1979-2019. *World Data Center for Climate (WDCC) at DKRZ*. https://doi.org/10.26050/WDCC/ESCiMo2_RD1SD.

Jöckel, P., Brinkop, S., Graf, P. Eichinger, R., Garny, H., Mertens, M., Nützel, M., Pozzer, A., 2024b: RD1SD: EMAC CCMI-2022 hindcast simulations with specified dynamics, ERA-5, 1979-2019 (additional data). *DOKU at DKRZ*. https://www.wdc-climate.de/ui/entry?acronym=DKRZ_LTA_853_dsg0002.

Kalakoski, N., Kujanpää, J., Sofieva, V., Tamminen, J., Grossi, M., and Valks, P., 2016: Validation of GOME-2/Metop total column water vapour with ground-based and in situ measurements. *Atmos. Meas. Tech.*, **9**, 1533–1544, https://doi.org/10.5194/amt-9-1533-2016.

Kang, M.-J. and Chun, H.-Y., 2021: Contributions of equatorial waves and small-scale convective gravity waves to the 2019/20 quasi-biennial oscillation (QBO) disruption, *Atmos. Chem. Phys.*, **21**, 9839–9857, https://doi.org/10.5194/acp-21-9839-2021.

Keppens, A., Lambert, J.-C., Granville, J., Hubert, D., Verhoelst, T., Compernolle, S., Latter, B., Kerridge, B., Siddans, R., Boynard, A., Hadji-Lazaro, J., Clerbaux, C., Wespes, C., Hurtmans, D. R., Coheur, P.-F., van Peet, J. C. A., van der A, R. J., Garane, K., Koukouli, M. E., Balis, D. S., Delcloo, A., Kivi, R., Stübi, R., Godin-Beekmann, S., Van Roozendael, M., and Zehner, C., 2018: Quality assessment of the Ozone_cci Climate Research Data Package (release 2017) – Part 2: Ground-based validation of nadir ozone profile data products. *Atmos. Meas. Tech.*, **11**, 3769–3800, https://doi.org/10.5194/amt-11-3769-2018.

Kinnersley, J. S. and Tung, K.-K., 1998: Modeling the global interannual variability of ozone due to the equatorial QBO and to extratropical planetary wave variability, *Journal of the Atmospheric Sciences*, Vol. **55**, 1417-1428, https://doi.org/10.1175/1520-0469(1998)055<1417:MTGIVO>2.0.CO;2.

Knowland, K. E., Wales, P. A., Wargan, K., Weir, B., Pawson, S., Damadeo, R., and Flittner, D., 2025: Stratospheric water vapor beyond NASA's Aura MLS: Assimilating SAGE III/ISS profiles for a continued climate record. *Geophysical Research Letters*, **52**, e2024GL112610, https://doi.org/10.1029/2024GL112610.

Koukouli, M. E., Valks, P., Poupkou, A., Zyrichidou, I., Rix, M., Hao, N., Katragkou, E., Balis, D., Loyola D., and Melas, D., 2013: Investigating the GOME2/MetopA Total Sulphur Dioxide Load with the Aid of Chemical Transport Modelling over the Balkan Region. In: Helmis, C., Nastos, P. (eds) *Advances in Meteorology, Climatology and Atmospheric Physics*. Springer Atmospheric Sciences. Springer, Berlin, Heidelberg. https://doi.org/10.1007/978-3-642-29172-2_150.

Koukouli, M. E., Balis, D. S., van der A, R. J., Theys, N., Hedelt, P., Richter, A., Krotkov, N., Li, C., and Taylor, M., 2016: Anthropogenic sulphur dioxide load over China as observed from different satellite sensors, *Atmospheric Environment*, **145**, 45-59, https://doi.org/10.1016/j.atmosenv.2016.09.007.

Lange, K., Richter, A., and Burrows, J. P., 2022: Variability of nitrogen oxide emission fluxes and lifetimes estimated from Sentinel-5P TROPOMI observations, *Atmos. Chem. Phys.*, **22**, 2745–2767, https://doi.org/10.5194/acp-22-2745-2022.

Latif, M., Anderson, D., Barnett, T., Cane, M., Kleeman, R., Leetmaa, A., O'Brien, J., Rosati, A., and Schneider, E., 1998: A review of the predictability and prediction of ENSO. *J. Geophys. Res.*, **103**(C7), 14375–14393, https://doi.org/10.1029/97JC03413.

Lelli, L., Kokhanovsky, A. A., Rozanov, V. V., Vountas, M., and Burrows, J. P., 2014: Linear trends in cloud top height from passive observations in the oxygen A-band. *Atmos. Chem. Phys.*, **14**, 5679–5692, https://doi.org/10.5194/acp-14-5679-2014.

Liu, S., Valks, P., Pinardi, G., De Smedt, I., Yu, H., Beirle, S., and Richter, A., 2019: An improved total and tropospheric NO_2 column retrieval for GOME-2. *Atmos. Meas. Tech.*, **12**, 1029–1057, https://doi.org/10.5194/amt-12-1029-2019.

Liu, S., Valks, P., Pinardi, G., Xu, J., Argyrouli, A., Lutz, R., Tilstra, L. G., Huijnen, V., Hendrick, F., and Van Roozendael, M., 2020: An improved air mass factor calculation for nitrogen dioxide measurements from the Global Ozone Monitoring Experiment-2 (GOME-2). *Atmos. Meas. Tech.*, **13**, 755–787, https://doi.org/10.5194/amt-13-755-2020.

Liu, S., Valks, P., Beirle, S., and Loyola, D. G., 2021: Nitrogen dioxide decline and rebound observed by GOME-2 and TROPOMI during COVID-19 pandemic. *Air Qual Atmos Health*, **14**, 1737–1755, https://doi.org/10.1007/s11869-021-01046-2.

Logan, J. A., Jones, D. B. A., Megretskaia, I. A., Oltmans, S. J., Johnson, B. J., Vömel, H., Randel, W. J., Kimani, W., and Schmidlin, F. J., 2003: Quasibiennial oscillation in tropical ozone as revealed by ozonesonde and satellite data, *J. Geophys. Res.*, **108**, D8, 4244, doi:10.1029/2002JD002170.

Loyola, D., Valks, P., Ruppert, T., Richter, A., Wagner, T., Thomas, W., van der A, R., and Meisner, R., 2006: The 1997 El Niño impact on clouds, water vapour, aerosols and reactive trace gases in the troposphere, as measured by the Global Ozone Monitoring Experiment, *Adv. Geosci.*, **6**, 267–272, https://doi.org/10.5194/adgeo-6-267-2006.

Loyola, D., van Geffen, J., Valks, P., Erbertseder, T., Van Roozendael, M., Thomas, W., Zimmer, W., and Wißkirchen, K., 2008: Satellite-based detection of volcanic sulphur dioxide from recent eruptions in Central and South America. *Adv. Geosci.*, **14**, 35–40, https://doi.org/10.5194/adgeo-14-35-2008.

Loyola, D. G., Coldewey-Egbers, R. M., Dameris, M., Garny, H., Stenke, A., Van Roozendael, M., Lerot, C., Balis, D., and Koukouli, M., 2009: Global long-term monitoring of the ozone layer – a prerequisite for predictions. *International Journal of Remote Sensing*, **30**(15–16), 4295–4318. https://doi.org/10.1080/01431160902825016.

Lu, Z., Schultze, A., Carré, M., Brierley, C., Hopcroft, P. O., Zhao, D., Zheng, M., Braconnot, P., Yin, Q., Jungclaus, J. H., Shi, X., Yang, H., and Zhang, Q., 2025: Increased frequency of multi-year El Niño–Southern Oscillation events across the Holocene, *Nature Geoscience*, **18**, 337–343, https://doi.org/10.1038/s41561-025-01670-y.

Millán, L., Santee, M. L., Lambert, A., Livesey, N. J., Werner, F., Schwartz, M. J., Pumphrey, H. C., Manney, G. L., Wang, Y., Su, H., Wu, L., Read, W. G., and Froidevaux, L., 2022: The Hunga Tonga-Hunga Ha'apai Hydration of the Stratosphere, *Geophysical Research Letters*, Volume **49**, Issue 13, e2022GL099381, https://doi.org/10.1029/2022GL099381.

Mitevski, I., Lee, S.H., Vecchi, G., Orbe, C., and Polvani, L. M., 2025: More positive and less variable North Atlantic Oscillation at high CO2 forcing, *npj Climate and Atmospheric Science*, **8**, 171, https://doi.org/10.1038/s41612-025-01051-7.

Newman, P. A., Coy, L., Pawson, S., and Lait, L. R., 2016: The anomalous change in the QBO in 2015–2016, *Geophys. Res. Lett.*, **43**, 8791–8797, doi:10.1002/2016GL070373.

Park, M., Randel, W. J., Kinnison, D. E., Bourassa, A. E., Degenstein, D. A., Roth, C. Z., McLinden, C. A., Sioris, C. E., Livesey, N. J., and Santee, M. L., 2017: Variability of stratospheric reactive nitrogen and ozone related to the QBO. *Journal of Geophysical Research: Atmospheres*, **122**, 10,103–10,118, https://doi.org/10.1002/2017JD027061.

Olsen, M. A., Wargan, K., and Pawson, S., 2016: Tropospheric column ozone response to ENSO in GEOS-5 assimilation of OMI and MLS ozone data, *Atmos. Chem. Phys.*, **16**, 7091–7103, https://doi.org/10.5194/acp-16-7091-2016.

Osprey, S. M., Butchart, N., Knight, J. R., Scaife, A. A., Hamilton, K., Anstey, J. A., Schenzinger, V., and Zhang, C., 2016: An unexpected disruption of the atmospheric quasi-biennial oscillation. *Science*, **353**, 1424–1427, doi:10.1126/science.aah4156.

Pinardi, G., Van Roozendael, M., Hendrick, F., Theys, N., Abuhassan, N., Bais, A., Boersma, F., Cede, A., Chong, J., Donner, S., Drosoglou, T., Dzhola, A., Eskes, H., Frieß, U., Granville, J., Herman, J. R., Holla, R., Hovila, J., Irie, H., Kanaya, Y., Karagkiozidis, D., Kouremeti, N., Lambert, J.-C., Ma, J., Peters, E., Piters, A., Postylyakov, O., Richter, A., Remmers, J., Takashima, H., Tiefengraber, M., Valks, P., Vlemmix, T., Wagner, T., and Wittrock, F., 2020: Validation of tropospheric NO_2 column measurements of GOME-2A and OMI using MAX-DOAS and direct sun network observations. *Atmos. Meas. Tech.*, **13**, 6141–6174, https://doi.org/10.5194/amt-13-6141-2020.

Pope, R. J., Chipperfield, M. P., Arnold, S. R., Glatthor, N., Feng, W., Dhomse, S. S., Kerridge, B. J., Latter, B. G., and Siddans, R., 2018: Influence of the wintertime North Atlantic Oscillation on European tropospheric composition: an observational and modelling study. *Atmos. Chem. Phys.*, **18**, 8389–8408, https://doi.org/10.5194/acp-18-8389-2018.

Punge, H. J. and Giorgetta, M. A., 2008: Net effect of the QBO in a chemistry climate model, *Atmos. Chem. Phys.*, **8**, 6505-6525, https://doi.org/10.5194/acp-8-6505-2008.

Randel, W. J., and Wu, F., 1996: Isolation of the ozone QBO in SAGE II data by singular-value decomposition, *Journal of the Atmospheric Sciences*, Vol. **53**, No. 17, 2546-2559.

Ravishankara, A. R., Daniel, J. S., and Portmann, R. W., 2009: Nitrous oxide (N_2O): The dominant ozone-depleting substance emitted in the 21s century, *Science*, Vol. **326**, 123–125, 10.1126/science.1176985.

Ribera, P., Peña-Ortiz, C., Garcia-Herrera, R., Gallego, D., Gimeno, L., and Hernández, E., 2004: Detection of the secondary meridional circulation associated with the quasi-biennial oscillation, *Journal of Geophysical Research Atmospheres*, Vol. **109**, D18112, https://doi.org/10.1029/2003JD004363.

Richter, J. H., Butchart, N., Kawatani, Y., Bushell, A. C., Holt, L., Serva, F., Anstey, J., Simpson, I. R., Osprey, S., Hamilton, K., Braesicke, P., Cagnazzo, C., Chen, C.-C., Garcia, R. R., Gray, L. J., Kerzenmacher, T., Lott, F., McLandress, C., Naoe, H., Scinocca, J., Stockdale, T. N., Versick, S., Watanabe, S., Yoshida, K., and Yukimoto, S., 2020: Response of the quasi-biennial oscillation to a warming climate in global climate models, *Quarterly Journal of the Royal Meteorological Society*, Volume **148**, Issue 744, 1490-1518, https://doi.org/10.1002/qj.3749.

Rix, M., Valks, P., Hao, N., Loyola, D., Schlager, H. Huntrieser, H., Flemming, J., Koehler, U. Schumann, U., and Inness, A., 2012: Volcanic SO_2, BrO and plume height estimations using GOME-2 satellite measurements during the eruption of Eyjafjallajökull in May 2010. *J. Geophys. Res.*, **117**, D00U19, doi:10.1029/2011JD016718.

Safieddine, S., Clerbaux, C., George, M., Hadji-Lazaro, J., Hurtmans, D., Coheur, P.-F., Wespes, C., Loyola, D., Valks, P., and Hao, N., 2013: Tropospheric ozone and nitrogen dioxide measurements in urban and rural regions as seen by IASI and GOME-2. *J. Geophys. Res. Atmos.*, **118**, 10,555–10,566, doi:10.1002/jgrd.50669.

Scannell, C., Hurtmans, D., Boynard, A., Hadji-Lazaro, J., George, M., Delcloo, A., Tuinder, O., Coheur, P.-F., and Clerbaux, C., 2012: Antarctic ozone hole as observed by IASI/MetOp for 2008–2010. *Atmos. Meas. Tech.*, **5**, 123–139, https://doi.org/10.5194/amt-5-123-2012.

Theys, N., Van Roozendael, M. Dils, B. Hendrick, F. Hao, N., and De Mazière, M., 2009: First satellite detection of volcanic bromine monoxide emission after the Kasatochi eruption. *Geophys. Res. Lett.*, **36**, L03809, doi:10.1029/2008GL036552.

Tian, W., Chipperfield, M. P., Gray, L. J., and Zawodny, J. M., 2006: Quasi-biennial oscillation and tracer distributions in a coupled chemistry-climate model, *Journal of Geophysical Research*, **111**, D20301, doi: 10.1029/2005JD006871.

Trenberth, K.E., Fasullo, J., and Smith, L., 2005: Trends and variability in column-integrated atmospheric water vapor, *Climate Dynamics*, **24**, 741-758, https://doi.org/10.1007/s00382-005-0017-4.

Trent, T., Schröder, M., Ho, S.-P., Beirle, S., Bennartz, R., Borbas, E., Borger, C., Brogniez, H., Calbet, X., Castelli, E., Compo, G. P., Ebisuzaki, W., Falk, U., Fell, F., Forsythe, J., Hersbach, H., Kachi, M., Kobayashi, S., Kursinski, R. E., Loyola, D., Luo, Z., Nielsen, J. K., Papandrea, E., Picon, L., Preusker, R., Reale, A., Shi, L., Slivinski, L., Teixeira, J., Vonder Haar, T., and Wagner, T., 2024: Evaluation of total column water vapour products from satellite observations and reanalyses within the GEWEX Water Vapor Assessment, *Atmospheric Chemistry and Physics*, **24**, 9667–9695, https://doi.org/10.5194/acp-24-9667-2024.

Tweedy, O. V., Kramarova, N. A., Strahan, S. E., Newman, P. A., Coy, L., Randel, W. J., Park, M., Waugh, D. W., and Frith, S. M., 2017: Response of trace gases to the disrupted 2015–2016 quasi-biennial oscillation, *Atmos. Chem. Phys.*, **17**, 6813–6823, https://doi.org/10.5194/acp-17-6813-2017.

Valks, P., Pinardi, G., Richter, A., Lambert, J.-C., Hao, N., Loyola, D., Van Roozendael, M., and Emmadi, S., 2011: Operational total and tropospheric NO_2 column retrieval for GOME-2. *Atmos. Meas. Tech.*, **4**, 1491–1514, https://doi.org/10.5194/amt-4-1491-2011.

Valks, P., Hao, N., Gimeno Garcia, S., Loyola, D., Dameris, M., Jöckel, P., and Delcloo, A., 2014: Tropical tropospheric ozone column retrieval for GOME-2. *Atmos. Meas. Tech.*, **7**, 2513–2530, https://doi.org/10.5194/amt-7-2513-2014.

van der A, R. J., Allaart, M. A. F., and Eskes, H. J., 2010: Multi sensor reanalysis of total ozone. *Atmos. Chem. Phys.*, **10**, 11277–11294, https://doi.org/10.5194/acp-10-11277-2010.

Van Loon, H., Zerefos, C. S., and Repapis, C. C., 1982: The southern oscillation in the stratosphere, *Mon. Weather Rev.*, **110**, 225-229.

Wang, Y., Rao, J., Lu, Y., Ju, Z., Yang, J., and Luo, J., 2023: A revisit and comparison of the quasi-biennial oscillation (QBO) disruption events in 2015/16 and 2019/20, *Atmospheric Research*, Volume **294**, 106970, https://doi.org/10.1016/j.atmosres.2023.106970.

Wargan, K., Weir, B., Manney, G. L., Cohn, S. E., Knowland, K. E., Wales, P. A., and Livesey, N. J. 2023: M2-SCREAM: A Stratospheric Composition Reanalysis of Aura MLS Data with MERRA-2 Transport. *Earth and Space Science*, **10**(2), e2022EA002632, https://doi.org/10.1029/2022EA002632.

Yook, S., Solomon, S., and Wang, X., 2025: The impact of 2022 hunga tonga-hunga ha'apai (hunga) eruption on stratospheric circulation and climate, *Journal of Geophysical Research: Atmospheres*, **130**, e2024JD042943, https://doi.org/10.1029/2024JD042943.

Zawodny, J. M., and McCormick, M. P., 1991: Stratospheric Aerosol and Gas Experiment II: Measurements of the quasi-biennial oscillation in ozone and nitrogen dioxide, *J. Geophys. Res.*, **96**, 9371–9377.

Zerefos, C. S., Van Loon, H., Repapis, C. C., 1982: Possible evidence of the southern oscillation in total ozone at Arosa. *Arch. Met. Geoph. Biocl. Ser. A*, **31**, 231-235.

Zerefos, C., Meleti, C., Balis, D., Tourpali, K., and Bais, A. F., 1998: Quasi-biennial and longer-term changes in clear sky UV-B solar irradiance, *Geophysical Research Letters*, Vol. **25**, No. 23, 4345-4348, 1998.

Zerefos, C. S., Eleftheratos, K., Kapsomenakis, J., Solomos, S., Inness, A., Balis, D., Redondas, A., Eskes, H., Allaart, M., Amiridis, V., Dahlback, A., De Bock, V., Diémoz, H., Engelmann, R., Eriksen, P., Fioletov, V., Gröbner, J., Heikkilä, A., Petropavlovskikh, I., Jarosławski, J., Josefsson, W., Karppinen, T., Köhler, U., Meleti, C., Repapis, C., Rimmer, J., Savinykh, V., Shirotov, V., Siani, A. M., Smedley, A. R. D., Stanek, M., and Stübi, R., 2017: Detecting volcanic sulfur dioxide plumes in the Northern Hemisphere using the Brewer spectrophotometers, other networks, and satellite observations. *Atmos. Chem. Phys.*, **17**, 551–574, https://doi.org/10.5194/acp-17-551-2017.

Zerefos, C., Kapsomenakis, J., Eleftheratos, K., Tourpali, K., Petropavlovskikh, I., Hubert, D., Godin-Beekmann, S., Steinbrecht, W., Frith, S., Sofieva, V., and Hassler, B., 2018: Representativeness of single lidar stations for zonally averaged ozone profiles, their trends and attribution to proxies. *Atmos. Chem. Phys.*, **18**, 6427–6440, https://doi.org/10.5194/acp-18-6427-2018.